

NAM

Advanced modelling of URM buildings in support of fragility and consequence functions derivation Using the Applied Element Method to model the collapse shake-table testing of a URM cavity wall structure

Daniele Malomo and Rui Pinho

Mosayk

Date October 2017

Editors Jan van Elk & Dirk Doornhof

General Introduction

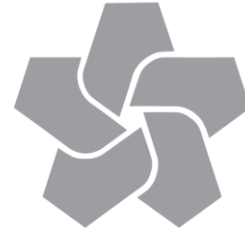
Many of the buildings in the Groningen field area are terraced unreinforced masonry buildings. A program to assess the response of these building to earthquakes was therefore initiated. This program built on the experimental and modelling program into the properties of URM building materials, wall elements and wall units.

A typical Groningen terraced house built using materials from the Groningen area by builders from the Groningen area, was tested at the shake-table of Eucentre in Pavia, Italy (Ref. 1). Although the building was at the end of this test program seriously damaged, the building had not collapsed. This left questions on the remaining capacity of the structure and its ability to resist larger seismic movements before (partially) collapsing. The test in Eucentre was therefore followed-up with further tests at the laboratory of LNEC in Lisbon, Portugal (Ref. 2 to 6). Here the upper floors of the building tested in Eucentre were re-built in the LNEC laboratory and subjected to movements measured at the base of the upper floors in Eucentre.

This report shows the results of modelling of the test in LNEC for the upper floors of the terraced building obtained by Mosayk using Extreme Loading for Structures (ELS), a commercial structural analysis software based on the Applied Element Method (AEM) after such tests, describing also the calibration process of the AEM numerical model.

References

1. Eucentre Shake-table Test of Terraced House Modelling Predictions and Analysis Cross Validation, staff from ARUP, Eucentre (Pavia) and TU Delft, November 2015 [this document also includes; (1) Instruments full-scale test-house Eucentre Laboratory, (2) Protocol for Shaking Table Test on Full Scale Building (Eucentre) V_1, and (3) Selection of Acceleration Time-Series for Shake Table Testing of Groningen Masonry Building at the EUCENTRE, Pavia, all three by staff from Eucentre (Pavia)],
2. Collapse shake-table testing of terraced house (LNEC-BUILD1), Eucentre and LNEC (U. Tomassetti, A. A. Correia, F. Graziotti, A.I. Marques, M. Mandirola, P.X. Candeias), 1st September 2017.
3. LNEC-BUILD1: Modelling predictions and analysis cross-validation, ARUP, TU Delft, Eucentre and Mosayk (several staff members from all four institutions), 8th September 2017.
4. Using the Applied Element Method to model the collapse shake-table testing of a URM cavity wall structure (LNEC-BUILD1), Mosayk (D. Malomo, R. Pinho), 31st October 2017.
5. Shake-table test up to collapse on a roof substructure of a Dutch terraced house (LNEC-BUILD2), Eucentre and LNEC (A.A. Correia, A.I. Marques, V. Bernardo, L. Grottoli, U. Tomassetti, F. Graziotti), 31st October 2017.
6. Using the Applied Element Method to model the collapse shake-table testing of a terraced house roof substructure (LNEC-BUILD2), Mosayk (D. Malomo, R. Pinho), 31st October 2017.



NAM

Title	Report on the v5 Fragility and Consequence Models for the Groningen Field		Date	October 2017
			Initiator	NAM
Autor(s)	Helen Crowley and Rui Pinho	Editors	Jan van Elk and Dirk Doornhof	
Organisation	Independent Academics	Organisation	NAM	
Place in the Study and Data Acquisition Plan	<p><u>Study Theme:</u> Development of Fragility Curves</p> <p><u>Comment:</u></p> <p>Crucially important for the assessment of seismic risk in the Groningen area are the fragility curves describing the response of the building stock and the consequence model describing the impact on life safety risk. The fragility curves describe the probability of exceedance of a given damage state for a building typology (structural system) in the Groningen field area depending on the ground motion.</p> <p>These fragility curves have been developed based on an experimental and modelling. The experimental program incorporates both in-situ and laboratory tests, to determine the properties of building materials, the behavior of wall elements and wall units and on tests of full-scale buildings. These tests have been conducted at the facilities of TU Delft TU Eindhoven, Eucentre (Pavia, Italy) and LNEC (Lisbon, Portugal). In these experiments much attention was given to masonry, but also pre-fab elements and pre-fab and cast-in-place concrete structures have been tested.</p> <p>The results of these experiments were used to model the seismic response of different structural systems (typologies) encountered in the Groningen building stock and further calibrate these models. Modelling was carried out by teams in ARUP, TU Delft, MOZAYK and Eucentre.</p> <p>Although much attention was given to unreinforced masonry building, cast-in-place concrete and pre-fab buildings have also been tested and modeled. Timber and steel frame buildings have also been studied and modelled. The hazard and risk assessment has been updated regularly (Ref. 1 to 4). Fragility curves used in these hazard and risk assessment of November 2015 (version 2) and for Winningsplan 2016 have been documented (Ref. 5). The current report describes the hazard and risk assessment version 5, used in the hazard and risk assessment of November 2017 (Ref. 6).</p>			
Directly linked research	<ul style="list-style-type: none"> (1) Building Material properties (2) Shake table tests (3) Seismic Response of Buildings (URM and non-URM) (4) Risk Assessment 			
Used data	Full experimental and Modelling program into seismic response URM & non-URM buildings.			
Associated organisation	NAM			
Assurance	Independent Assurance Panel			

D6

DELIVERABLE

Project Information

Project Title: **Advanced modelling of URM buildings in support of fragility/consequence functions derivation**

Project Start: May 2016

Duration: 20 months

Technical Point of Contact: Rui Pinho

Administrative Point of Contact: Roberto Nascimbene

Deliverable Information

Deliverable Title: **Using the Applied Element Method to model the collapse shake-table testing of a URM cavity wall structure**

Data of Issue: 31st October 2017

Author: Daniele Malomo

Reviewer: Rui Pinho

REVISION: **v1**

Table of Contents

Executive Summary	4
Nomenclature	5
1 Introduction	6
1.1 Scope	6
1.2 Analysis method.....	6
1.3 Building prototype.....	6
1.4 Mechanical properties of masonry	7
1.5 Testing procedure	7
2 Brief Overview of Test Specimen Response	9
3 Blind Prediction Modelling	10
3.1 Preliminary numerical model	10
3.2 Preliminary material properties	11
3.3 Summary of results.....	11
3.4 Floor hysteresis.....	14
3.5 Roof acceleration hysteresis.....	14
3.6 Global hysteresis.....	14
3.7 Crack patterns and collapse mechanism	15
4 Post-Test Refined Modelling	17
4.1 Numerical model.....	17
4.2 Post-test material properties	18
4.3 Summary of results.....	19
4.4 Floor hysteresis.....	21
4.5 Roof acceleration hysteresis.....	23
4.6 Global hysteresis.....	24
4.7 Crack patterns and collapse mechanism	26
5 Closing Remarks	29
References	30
Appendix A – further details on URM model building in ELS	31
A.1 AEM modelling of contact surfaces between elements.....	31
A.1.1 Nailed connections between beam and plank elements.....	32
A.1.2 Definition of “weak” and “cracked” mortar spring interfaces	34
A.2 Numerical modelling of plank elements.....	35
A.3 Connectors, ties and steel anchors elements	37

A.4 Derivation of mortar Young’s modulus from homogenisation formulae..... 38
A.5 References 40

Executive Summary

A full-scale URM cavity wall house specimen (LNEC-BUILD1) was tested in 2017 at the shake-table of the Laboratório Nacional de Engenharia Civil (LNEC - Lisbon, Portugal) under the coordination of the European Centre of Training and Research in Earthquake Engineering (Eucentre - Pavia, Italy). The test was carried out within the framework of the research programme on hazard and risk of induced seismicity in the Groningen region, sponsored by the Nederlandse Aardolie Maatschappij BV (NAM).

In tandem with such experimental endeavour, a blind-prediction modelling exercise was also undertaken, involving four different modelling teams, each of which employing markedly diverse structural modelling strategies and tools. Mosayk was one of such teams, modelling the test specimen using Extreme Loading for Structures (ELS), a commercial structural analysis software based on the Applied Element Method (AEM).

This report shows the results obtained by Mosayk both before (blind prediction) as well as after (calibrated post-diction) the test, describing also the calibration process of the AEM numerical model. It is shown how both the pre- and post-test models are representative of the actual behaviour of the test specimen in terms of average displacement and global capacity, whilst refined post-test model was also able to reproduce the collapse mechanism observed during the test.

Nomenclature

Symbol	Description
ρ	Mass density [kg/m^3]
E	Masonry Young's modulus [MPa]
E_{mo}	Mortar Young's modulus [MPa]
E_{u}	Unit Young's modulus [MPa]
ν	Poisson's ratio of masonry
f_{m}	Masonry compressive strength [MPa]
f_{w}	Flexural bond strength of mortar joints [MPa]
f_{v0}	Masonry (bed joint) initial shear strength (cohesion) [MPa]
μ	Masonry (bed joint) shear friction coefficient

1 Introduction

1.1 Scope

The test specimen (LNEC-BUILD1) built in the LNEC laboratory in Lisbon is a full-scale one-storey building, with a timber roof and RC slab, corresponding to the second floor and roof of the URM cavity wall terraced house specimen tested in the Eucentre laboratory in 2015 (EUC-BUILD1, see report by Graziotti et al., 2015). For this reason, the seismic input introduced at the base of LNEC-BUILD1 specimen corresponded to the floor accelerations that had been recorded during the EUC-BUILD1 test; further details can be found in the corresponding test report (Tomassetti et al., 2017a).

In addition to enhance further the knowledge of the dynamic response of this type of structures by testing it all the way up to collapse, the main goal of the LNEC-BUILD1 experimental endeavour was that of allowing the assessment of the capability of available numerical modelling approaches in predicting the ultimate collapse capacity of these URM cavity wall terraced houses.

As such, a blind-prediction modelling exercise was undertaken, involving four different modelling teams, each of which employing markedly diverse structural modelling strategies and tools (see report by Arup, 2017). Mosayk was one of such teams, modelling the test specimen using ELS - Extreme Loading for Structures (ASI, 2017), a commercial structural analysis software based on the Applied Element Method (Meguro and Tagel-Din, 2000, 2001, 2002). This report thus describes such modelling effort by Mosayk.

1.2 Analysis method

According to the Applied Element Method (AEM), a given structure is discretised as a virtual assembly of small rigid units, carrying only mass and damping of the system, connected by linear and nonlinear springs (with normal stiffness k_n and shear stiffness k_s) in which the material properties are lumped. It is noted that, even if the single mesh element is rigid, the behaviour of the whole assembly is deformable. Thus, a masonry wall segment can be represented by means of units (fully rigid or deformable) linked by dimensionless mortar layers (simplified micro-modelling). The theoretical formulation allows reproducing the structural response both in the finite and discrete numerical domains, taking into account contacts and dynamic element interactions automatically. In addition to the pioneering publications listed above, further details on the AEM formulation may be found in e.g. Mosayk (2016) and Malomo (2018).

1.3 Building prototype

The LNEC-BUILD1 prototype was 5.82 m long, 5.46 m wide and 4.93 m high with a total mass of 31 t. The cavity-wall system consisted in an inner loadbearing leaf made of calcium silicate (CS) bricks (supporting the first floor reinforced concrete slab) whereas the external leaf was a clay brick (CL) veneer without any loadbearing function. The two gable walls in the transverse façades (East and West) supported a 43° pitched timber roof. An air gap of 80 mm was left between the two leaves, as usually seen in common practice. Steel ties with a diameter of 3.1 mm and a length of 200 mm were inserted in the mortar layers during construction, ensuring the connection between the two masonry leaves. Finally, it is important to note that the slab was not directly supported by the CS longitudinal walls. Indeed, the gap between the slab and the inner CS longitudinal walls was filled with mortar after the removal of the temporary supports and the attainment of the slab's deflection resulting in almost no vertical load being transmitted to the longitudinal walls under static conditions. Further details can be found in Tomassetti et al. (2017a).

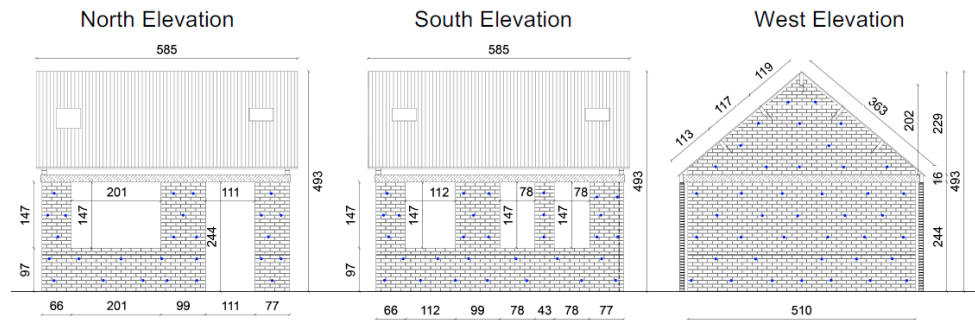


Figure 1 Elevation views of the specimen's CS inner leaf (Tomassetti et al., 2017a)

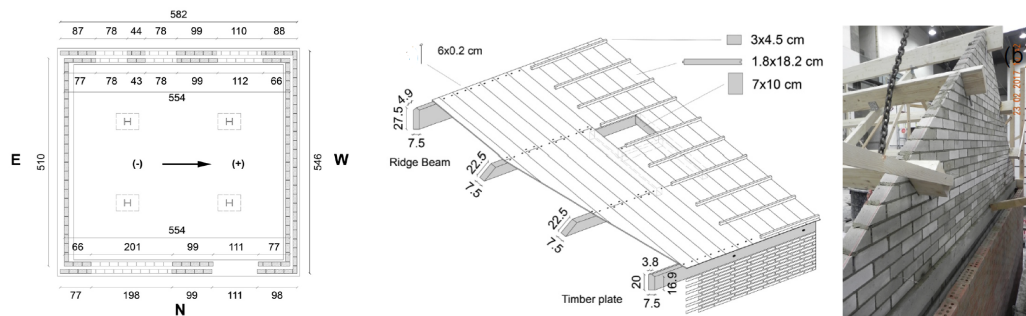


Figure 2 Plan view of the ground floor (left) and details of roof structure (right) (Tomassetti et al., 2017a)

1.4 Mechanical properties of masonry

Both CS and CL masonry components were tested at Eucentre and LNEC in order to characterise the masonry material and obtain the mechanical properties reported in Table 1, below. The “preliminary material properties” refer to the values available during the blind prediction modelling exercise (April 2017), whereas the “post-test material properties” are those parameters considered for the post-test refined simulations (August 2017).

Table 1 Preliminary and post-test material properties

Symbol	Preliminary material properties		Post-test material properties	
	CS	CL	CS	CL
ρ	1835	1905	1800	1839
E	4000 ¹	6000 ¹	7955 ¹	3535 ¹
E_{mo}	---	---	---	---
E_u	8990	7211	8990	7211
ν	---	---	---	---
f_m	7	12	9.80	19.39
f_w	0.39	0.25	0.36	0.25
f_{v0}	0.27	0.17	0.45	0.41
μ	0.45	0.68	0.48	0.75

¹ Secant stiffness to 33% f_m

1.5 Testing procedure

The building specimen constructed on the shake-table of LNEC was subjected to incremental dynamic tests, i.e. a series of shake-table runs under input motions of increasing intensity up to collapse of the structure. Two different ground motions had been originally selected for the EUC-BUILD1 test, EQ1 and EQ2 (Graziotti et al., 2015). The second floor response acceleration time-histories recorded during the test of EUC-BUILD1 for both EQ1 and EQ2 were then imposed at the

ground floor of LNEC-BUILD1. In Figure 3 below the considered acceleration time-histories are reported. The sequence of the input motions, the relative scaled factors applied and the associated horizontal and vertical peak ground accelerations (PGA) are summarised in Table 2. It is noted that, because of technical issues (refer to Tomassetti et al., 2017a), the loading sequence initially planned was altered during the test by adding or removing different seismic inputs, as reported in Table 2 below.

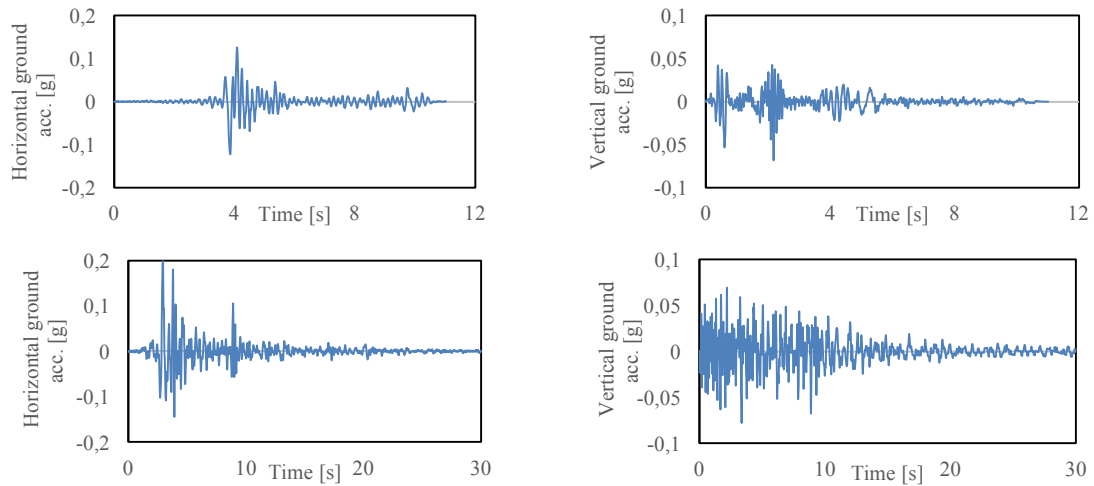


Figure 3 EQ1@100 horizontal (left) and vertical (right) seismic inputs

Table 2 LNEC-BUILD1 test sequence (P=planned, A=actual input)

Seq-n°	Test ID	Hor.PGA [g]		Ver.PGA [g]		Seq-n°	Test ID	Hor.PGA [g]		Ver.PGA [g]	
		P	A	P	A			P	A	P	A
1	EQ1@25	0.04	-	0.02	-	9	EQ2@150	0.28	0.38	0.12	0.21
2	EQ1@50	0.08	0.06	0.03	0.04	10	EQ2@60	-	0.13	-	0.05
3	EQ1@100	0.13	0.12	0.07	0.08	11	EQ2@120	-	0.30	-	0.13
4	EQ1@150	0.17	0.15	0.10	0.12	12	EQ2@200	0.33	0.39	0.16	0.18
5	EQ2@50a	-	0.14	-	0.05	13	EQ2@250	0.40	-	0.20	-
6	EQ2@50b	0.11	0.10	0.04	0.07	14	EQ2@300	0.47	0.63	0.23	0.34
7	EQ2@100	0.20	0.22	0.08	0.10	15	EQ2@400	0.61	0.63	0.23	0.34
8	EQ2@125	0.23	-	0.10	-	-	-	-	-	-	-

2 Brief Overview of Test Specimen Response

For technical reasons, the LNEC-BUILD2 specimen could not be constructed directly on the shake-table. During the transportation phase, and as reported in Tomassetti et al. (2017a), the structure suffered slight damage prior the test execution. In Figure 4 below, the associated cracks are depicted.

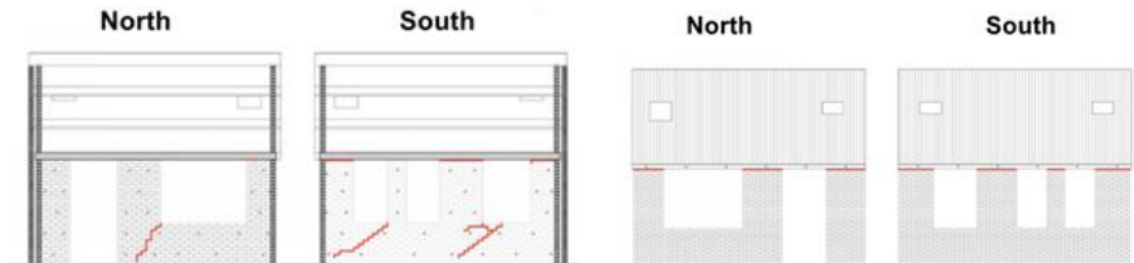


Figure 4 Damage suffered by the specimen during transportation phase; inner CS leaf (right) and outer CL walls (left)

Concerning the test, no relevant damage was detected until EQ1@150, when the front/back inner CS leafs started rocking. During EQ2@150 the cracks previously developed continued to propagate through the CS elements, and EQ2@200 was characterised by the out-of-plane (OOP) damage occurred to the North CS wall, mainly due to the so-called flange-effect. At this stage, the CL walls suffered only slight damage located at the interface with the wooden beams.

During EQ2@300, an OOP mechanism of the South CS wall occurred, and the test was stopped. This phenomenon was associated to the loss of boundary conditions of the wall, due to the RC slab uplift caused by the increase in the rocking demand of the longitudinal piers. The structure at this stage suffered severe damage to the North, East and West CS walls as well. The CL piers, instead, exhibited only localised damage to the base of the longitudinal piers, a continuous straight crack (corresponding to the slab level) and a stepped crack to the North wall (see Figure 5).

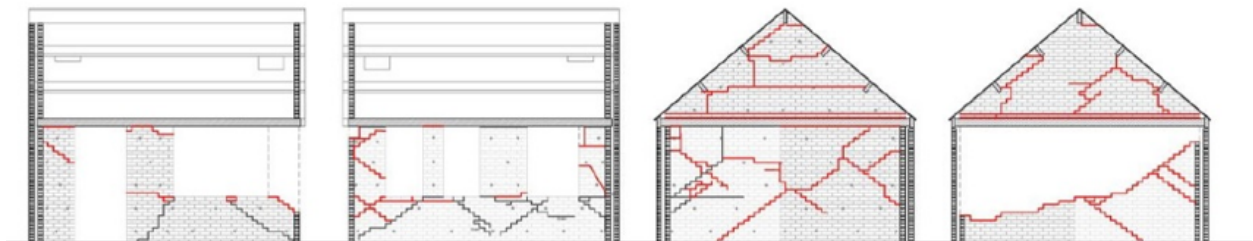


Figure 5 Damage detected at the end of EQ@300 to the East, West, North and South CS inner walls respectively

More details about the experimental procedure and the specimen response can naturally be found in the dedicated test report by Tomassetti et al. (2017a). In what follows, the most relevant experimental results are shown and compared to the numerical results obtained with the analyses carried out prior and after the test.

3 Blind Prediction Modelling

In this section, a brief overview of the results obtained before the test is included. It is noted that, as already stated, since the initially planned input motions and the actual ones are slightly different, a detailed comparison (e.g. scrutinising the structural response or the damage for each input) cannot be strictly carried out. However, the comparison of the global response in terms of hysteretic behaviour, reported in what follows, does manage to provide a general idea of the reliability of the numerical model.

3.1 Preliminary numerical model

The most relevant modelling assumptions related to the numerical model assembled prior to the test (depicted in Figure 6) are briefly summarised in Table 3.

Table 3 Modelling assumptions

Input	Modelling assumption
Boundary condition	Structure connected by mortar interfaces to a fixed slab
Roof diaphragm	Nailed connection between planks and beams modelled as equivalent spring interfaces characterised by an elastic-perfectly-plastic behaviour
Wall ties	Elastic-perfectly-plastic beam elements
Attic floor slab and front/back inner leaves connection	Mortar interface (active after the static/gravity loading stage)
Timber beam and front/back outer leaves connection	Mortar interface (active after the static/gravity loading stage)
Attic floor slab and end/party walls connection	Mortar interface
Connection between roof girders and end/party walls	Mortar interface plus elastic-perfectly plastic L-steel anchors

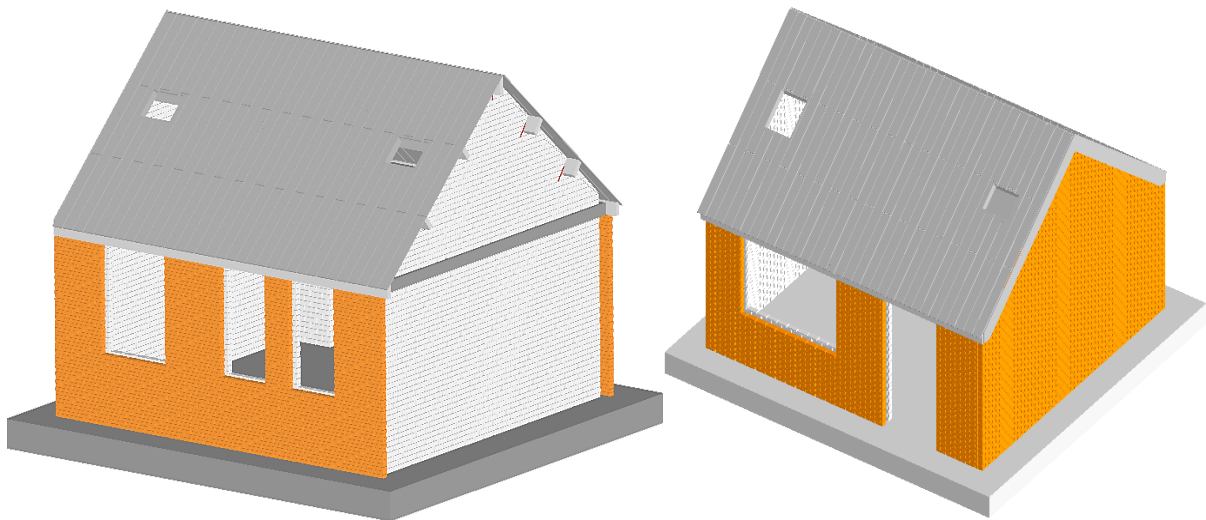


Figure 6 Screenshots of the preliminary numerical model

It is also noted that, in order to decrease the computational burden, the bricks were assumed to be rigid and the number of springs was reduced. Thus, mechanisms that involve the deformability of bricks, such as crushing of masonry due to the splitting of the unit, cannot be taken into account, which may result in a lower prediction of energy dissipation. Furthermore, it is noted that the gravity contribution of the roof tiles was modelled through a system of lumped masses shared

amongst the elements of the mesh, again with the aim at reducing the calculation steps, resulting in a potentially slightly altered acceleration demand at the roof structure. Finally, the mortar properties were inferred by empirical formulae; from previous modelling experiences, this might imply that the model could exhibit a more flexible response than the experimental one.

3.2 Preliminary material properties

In Table 4 and Table 5 below, the material characterization test values as well as values assumed for the blind prediction for both CS and CL masonry are reported.

Table 4 CS masonry preliminary characterisation test and numerical properties

Symbol	Description	Preliminary test value ¹	ELS
ρ	Mass density [kg/m ³]	1835	1835
E	Masonry Young's modulus [MPa]	4000 ²	---
E _{mo}	Mortar Young's modulus [MPa]	---	997 ³
E _u	Unit Young's modulus [MPa]	8990	8990
ν	Poisson's ratio of masonry	---	0.25
f _m	Masonry compressive strength [MPa]	7	7
f _w	Flexural bond strength of mortar joints [MPa]	0.39	0.39
f _{v0}	Masonry (bed joint) initial shear strength (cohesion) [MPa]	0.27	0.27
μ	Masonry (bed joint) shear friction coefficient	0.45	0.45

Table 5 CL masonry preliminary characterisation test and numerical properties

Symbol	Description	Preliminary test value ¹	ELS
ρ	Mass density [kg/m ³]	1905	1905
E	Masonry Young's modulus [MPa]	6000 ²	---
E _{mo}	Mortar Young's modulus [MPa]	---	3039 ³
E _u	Unit Young's modulus [MPa]	7211	7211
ν	Poisson's ratio of masonry	---	0.25
f _m	Masonry compressive strength [MPa]	12	12
f _w	Flexural bond strength of mortar joints [MPa]	0.24	0.24
f _{v0}	Masonry (bed joint) initial shear strength (cohesion) [MPa]	0.17	0.17
μ	Masonry (bed joint) shear friction coefficient	0.68	0.68

¹ Based on tentative mechanical characteristics of masonry material provided by Eucentre (Tomassetti et al., 2017b)

² Secant stiffness to 33%*f_m*

³ Inferred by means of empirical formulae (Ciesielski 1999; ICBO 1991; Matysek and Janowski 1996; Brooks and Baker 1998)

3.3 Summary of results

The numerical outcomes obtained are summarised below, representing the envelope plots and deflected shape prior to collapse.

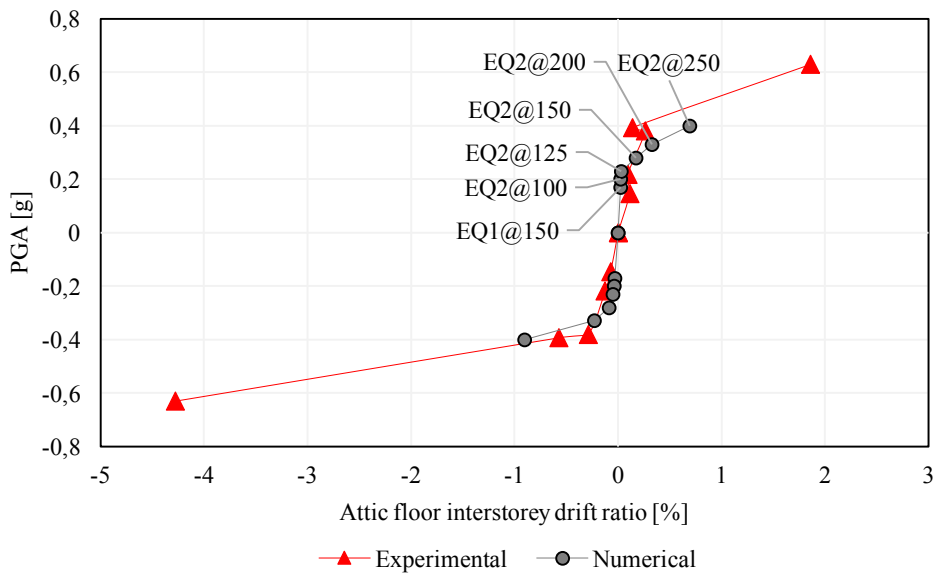


Figure 7 IDA: PGA vs attic floor IDR¹

¹ PGA vs. attic floor interstorey drift ratio (IDR) IDA curve plots the PGA [g] vs. the positive and negative direction IDR envelopes of attic floor [%] for each test.

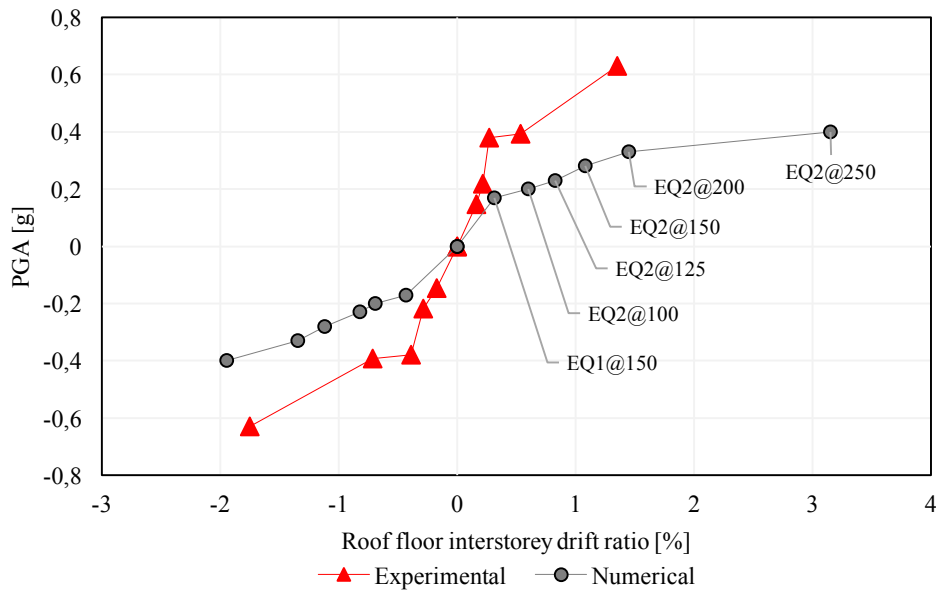


Figure 8 IDA: PGA vs roof floor IDR¹

¹ PGA vs. roof interstorey drift ratio (IDR) IDA curve plots the PGA [g] vs. the positive and negative direction IDR envelopes of roof [%] for each test.

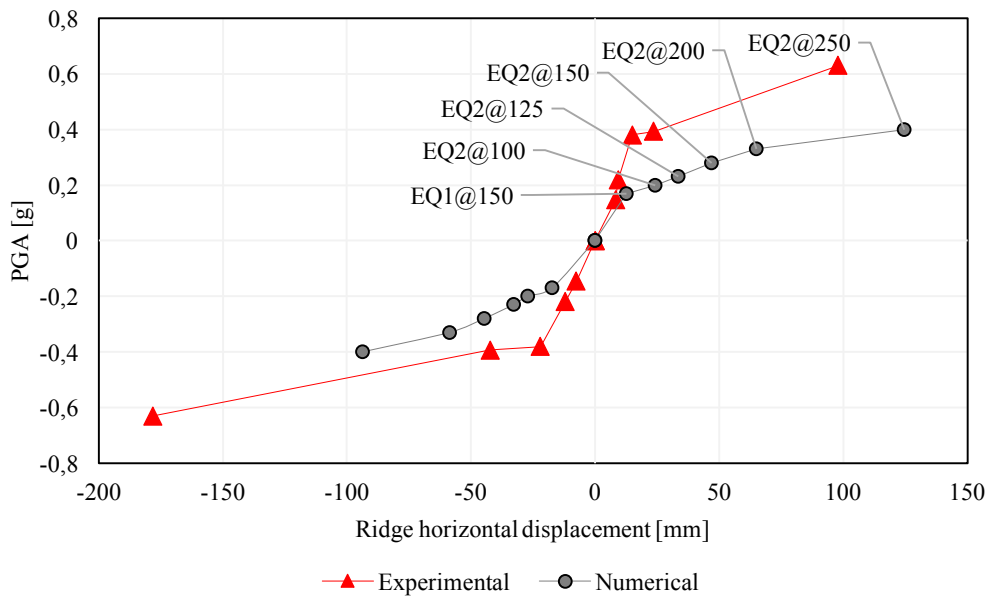


Figure 9 IDA: PGA vs ridge displacement¹

¹ PGA vs. ridge displacement is defined as the PGA [g] vs. the positive and negative direction displacement envelopes of the ridge relative to the base [mm] for each test

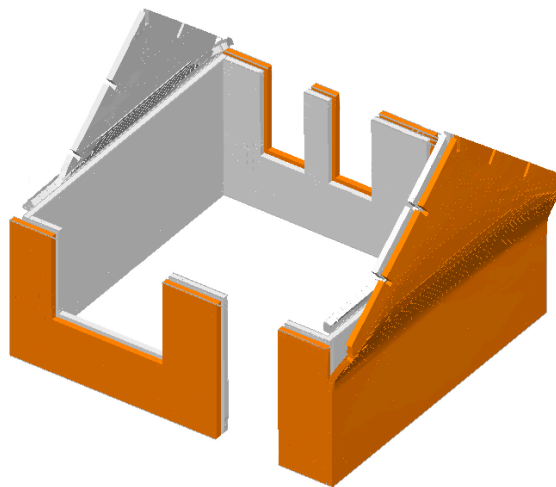


Figure 10 Deflected shape at collapse

In the subsequent sub-Sections, the comparison between the numerical and experimental hysteretic response in terms of both floor displacement and ridge acceleration is investigated. It is recalled that, since the experimental loading protocol was slightly different from the one initially planned (and consequently employed for the blind prediction analyses), the experimental hysteresis (in grey) reported below are referred to the final lab input (i.e. EQ2@300), whilst the numerical model hysteretic behaviour (in black), instead predicted collapse at EQ2@250 (not performed during the test, as gathered from Table 2).

3.4 Floor hysteresis

Floor hysteresis is defined as the total “base” shear [kN] vs. attic floor horizontal displacement relative to the base [mm]. Grey is experimental and black is numerical.

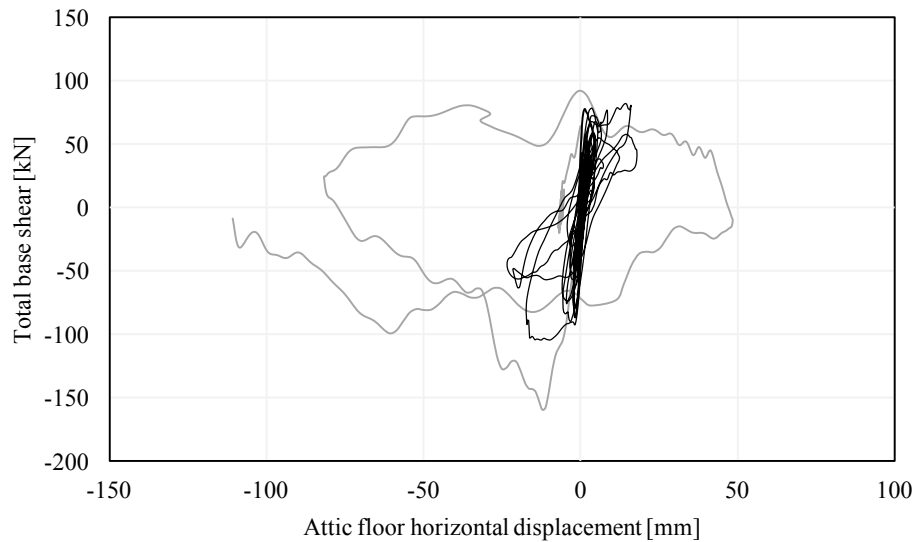


Figure 11 Base shear vs floor horizontal displacement

3.5 Roof acceleration hysteresis

Roof [acceleration] hysteresis is defined as the ridge horizontal acceleration [g] vs. ridge horizontal displacement relative to the attic floor horizontal displacement [mm].

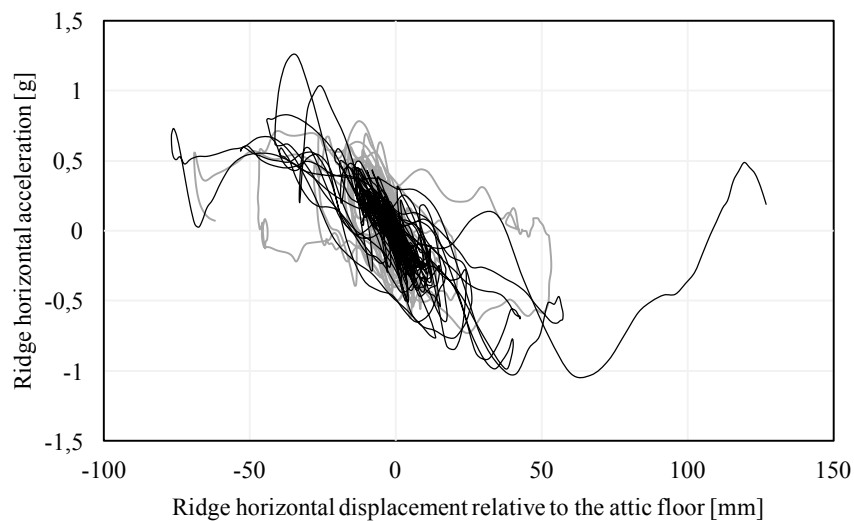


Figure 12 Base shear vs ridge horizontal displacement relative to the attic floor

3.6 Global hysteresis

Global hysteresis is defined as the total “base” shear [kN] vs. ridge horizontal displacement relative to the base [mm].

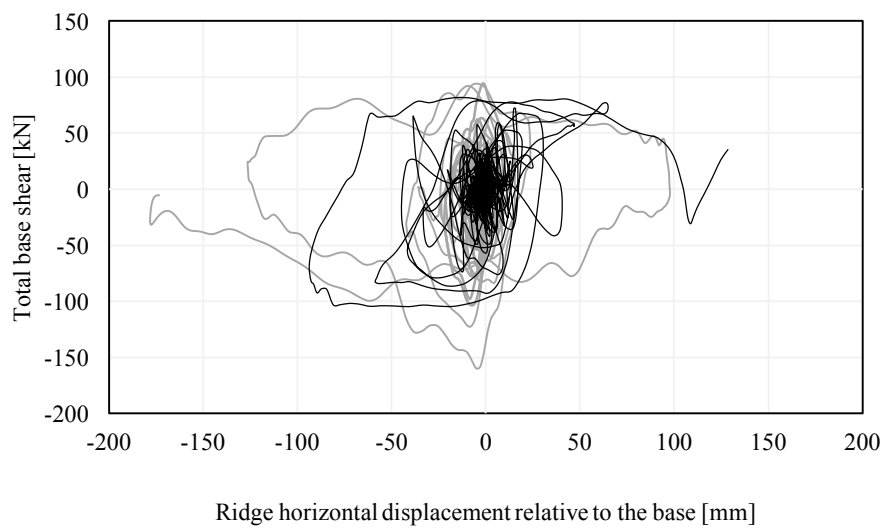


Figure 13 Base shear vs ridge horizontal displacement relative to the base

3.7 Crack patterns and collapse mechanism

The main failure mechanisms predicted by the preliminary numerical model are summarised below:

- Gables overturning (first damage: end of EQ1_150)
- Flexural mechanisms of the slender piers (first significant damage: EQ2_125)
- Out-of-plane mechanism of the inner party wall and the outer leaf end wall (EQ2_150)

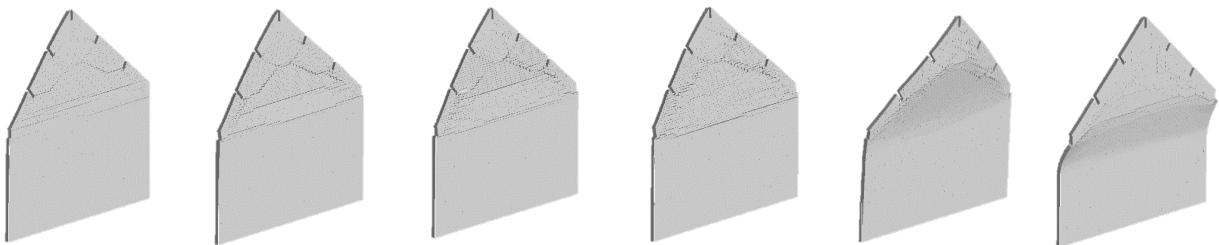


Figure 14 Damage evolution of the North outer leaf wall from EQ1_150 to EQ2_250 (varied magnification)

With the exception of the gables, the model did not predict any noticeable damage during the analysis under the first seismic excitations (i.e. up until EQ1 150% - 0.17g), and only slight damage appeared after the test under 125% of EQ2 (0.23g), mainly involving the inner leaf wall on the West side and the outer leaf walls on the East and West side. The gables exhibited stepped cracks along the areas of influence of the external reinforcement (the L-shape steel anchors on the South side and the timber barge board on the North side at roof level) already at the end of the sequence of EQ1.

The response of the interfaces between the RC slab and the longitudinal walls was characterised by an almost uniform sliding failure at EQ2 150% (0.28g) corresponding to a 1st inter-storey drift of 0.18%. During EQ2 150% and EQ2 200% (0.33g) the diagonal cracks between the longitudinal walls and the spandrels become significant and indicative of the pier's flexural response. The damage of both the 1st storey transversal walls was relatively negligible until EQ2 200% for the outer leaf end wall. Light damage only was observed in the inner leaf end wall, mainly located at the interface with the slab. During EQ2 150% and EQ2 200%, a substantial increase in the out-of-

plane damage of both gables was predicted, leading to an almost simultaneous collapse of the upper-portion of the structure at one-third of EQ2 250% (0.40g).

As it is clear from observing Figure 14 above, the governing mode of failure exhibited by the preliminary numerical model is the overturning of the South gable, whereas the test specimen experienced the collapse of the CS party wall due to the RC slab uplift. However, with the exception of the experimental response of the last seismic input (that was not modelled, as already stated) and given the differences in terms of loading protocol, the blind pre-test numerical model can be deemed as having been able to adequately predict the overall capacity and simulate both the displacement and the acceleration demand of the attic floor and the ridge beam respectively.

4 Post-Test Refined Modelling

4.1 Numerical model

The loading protocol of the post-test refined numerical model has been modified with the aim to reduce the computational burden. Indeed, the final portion of each ground motion was truncated. Moreover, for the same reason, the discretisation of several elements (including the RC slab, beams and planks) was consistently reduced.

Although the main structure of the previous model was substantially maintained, some relevant improvements were introduced:

- Updated material properties
- Enhanced modelling of the interfaces between adjacent walls
- Introduced pre-cracked interfaces between longitudinal walls and beams/slab

The most relevant modelling assumptions related to the numerical model built after the test are briefly summarised in Table 6 below, and subsequently explained and justified in further detail (see also Appendix A).

Table 6 Modelling assumptions (changes with respect to pre-test model are indicated in bold characters)

Input	Modelling assumption
Boundary condition	Structure connected by mortar interfaces to a fixed slab
Roof diaphragm	Nailed connection between planks and beams modelled as equivalent spring interfaces characterised by an elastic-perfectly-plastic behaviour
Wall ties	Elastic-perfectly-plastic beam elements
Attic floor slab-front/back inner leaves connection	Cracked mortar interface accounting for the damage occurred during transportation phases (active after the static/gravity loading stage)
Timber beam-front/back outer leaves connection	Cracked mortar interface accounting for the damage occurred during transportation phases (active after the static/gravity loading stage)
Attic floor slab and end/party walls connection	Mortar interface
Connection between roof girders and end/party walls	Mortar interface plus elastic-perfectly plastic L-steel anchors
Wall-to-wall connection	45-degrees connections between adjacent walls (see Figure 15(c))

The material properties of both CS and CL masonry were updated in light of the data provided by the characterisation tests, as reported in Tomassetti et al. (2017). The geometrical connections between wall elements were further investigated in order to evaluate their influence on both in-plane and out-of-plane structural response. The wall-to-wall connections were subsequently modified, and a 45-degrees interface joint (see Figure 15c) was adopted for both CS and CL walls.

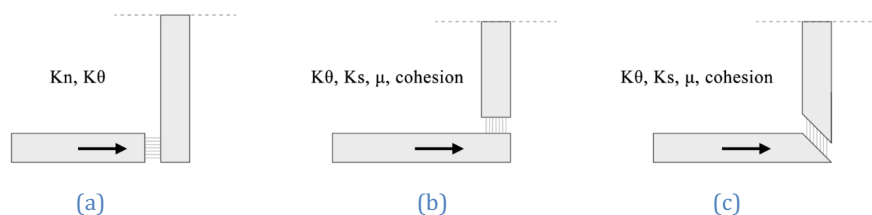


Figure 15 (a) (b) (c) Different types of wall-to-wall connections that may be employed with the AEM

Different values of tensile strength (i.e. direct and flexural bond strength) were used in the model for longitudinal and transverse walls, as well as for the wall-to-wall connections, which were based on the expected structural behaviour. Furthermore, the interface between the wooden beams and the longitudinal CS walls was modelled using a pre-cracked mortar material in order to match the initial conditions of the specimen.

Finally, and as mentioned at the start of this Section, it is also noted that the final portion of each of the two accelerograms was truncated (obtaining a duration of 6s for EQ1 and of 10s for EQ2). This approach consistently reduced the computational time, and no relevant differences with the “complete” (i.e. with non-truncated inputs) models were noticed.

4.2 Post-test material properties

In Table 7 and Table 8 below, the final material characterisation test values, as well as values assumed for the post-test prediction for both CS and CL masonry, are reported.

Table 7 CS masonry post-test characterisation test and numerical properties (in bold values that were updated)

Symbol	Description	Test value ⁴	Blind	Post-Test
ρ	Mass density [kg/m ³]	1800	1835 ²	1835
E	Masonry Young's modulus [MPa]	7955 ¹	---	---
E _{mo}	Mortar Young's modulus [MPa]	---	997 ^{2,3}	4537
E _u	Unit Young's modulus [MPa]	8990	8990	8990
ν	Poisson's ratio of masonry	---	0.25	0.25
f _m	Masonry compressive strength [MPa]	9.8	---	---
f _{mo}	Mortar compressive strength [MPa]	6.20	16.3	16.3
f _u	Brick compressive strength [MPa]	16.3	16.3 ²	16.3
f _w	Flexural bond strength of mortar joints [MPa]	0.36	0.39 ²	0.36
f _t	Tensile strength of mortar joints [MPa]	---	---	0.85⁴
f _{v0}	Masonry (bed joint) initial shear strength (cohesion) [MPa]	0.45	0.27 ²	0.45
μ	Masonry (bed joint) shear friction coefficient	0.48	0.45 ²	0.48

Table 8 CL masonry post-test characterisation test and numerical properties (in bold values that were updated)

Symbol	Description	Test value ⁴	Blind	Post-Test
ρ	Mass density [kg/m ³]	1839	1905 ²	1905 ²
E	Masonry Young's modulus [MPa]	13118 ¹	---	---
E _{mo}	Mortar Young's modulus [MPa]	---	3039 ^{2,3}	3535
E _u	Unit Young's modulus [MPa]	7211	7211	7211
ν	Poisson's ratio of masonry	---	0.25 ⁴	0.25
f _m	Masonry compressive strength [MPa]	19.39	---	----
f _{mo}	Mortar compressive strength [MPa]	8.34	32.45	32.45
f _u	Brick compressive strength [MPa]	32.45	32.45	32.45
f _w	Flexural bond strength of mortar joints [MPa]	0.19	0.25 ⁴	0.25
f _t	Tensile strength of mortar joints [MPa]	---	---	0.98⁴
f _{v0}	Masonry (bed joint) initial shear strength (cohesion) [MPa]	0.41	0.17 ²	0.41
μ	Masonry (bed joint) shear friction coefficient	0.75	0.68 ²	0.75

¹ Secant stiffness to 33% f_m

² Based on preliminary blind-prediction estimations

³ Inferred by means of empirical formulae (Ciesielski 1999; ICBO 1991; Matysek and Janowski 1996; Brooks and Baker 1998)

⁴ Inferred by means of empirical formulae (Kim and Reda Taha, 2014)

4.3 Summary of results

The numerical outcomes obtained are summarised below, in the form of hysteresis envelope plots and deflected shape prior to collapse.

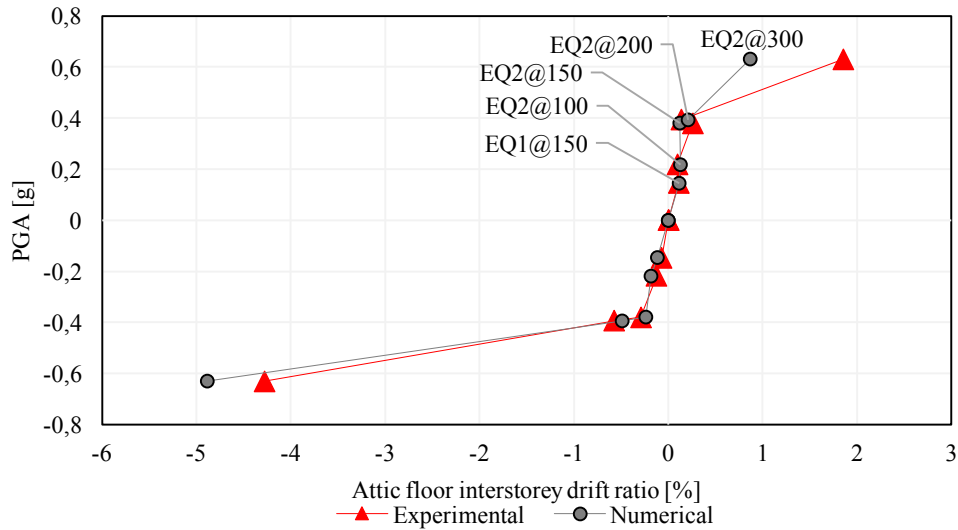


Figure 16 IDA: PGA vs attic floor IDR¹

¹ PGA vs. attic floor interstorey drift ratio (IDR) IDA curve plots the PGA [g] vs. the positive and negative direction IDR envelopes of attic floor [%] for each test.

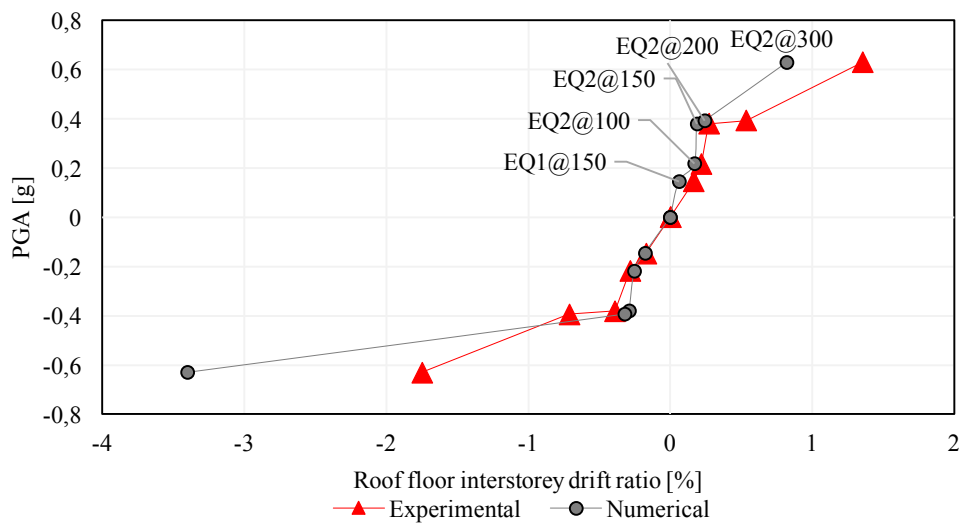


Figure 17 IDA: PGA vs roof floor IDR¹

¹ PGA vs. roof interstorey drift ratio (IDR) IDA curve plots the PGA [g] vs. the positive and negative direction IDR envelopes of roof [%] for each test.

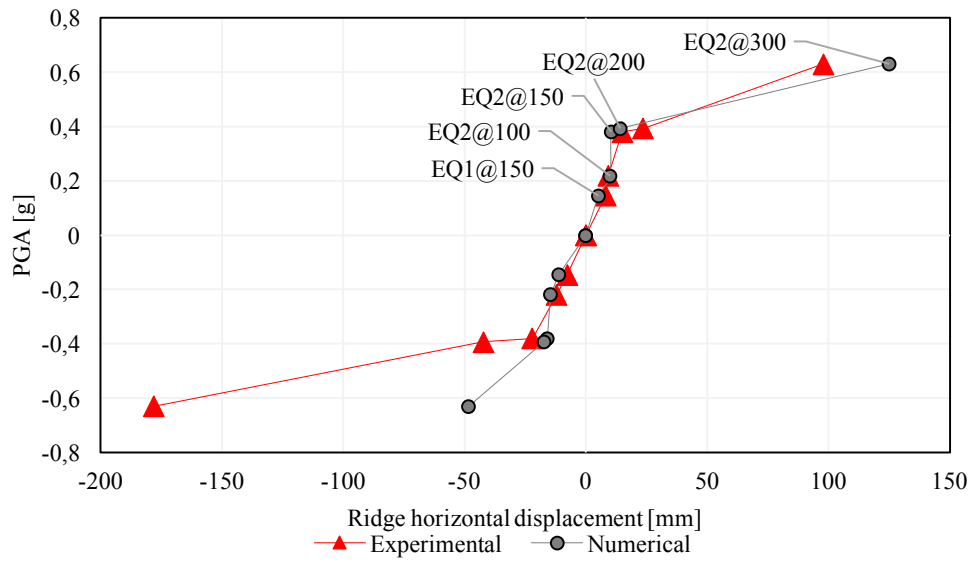


Figure 18 IDA: PGA vs ridge displacement ¹

¹ PGA vs. ridge displacement is defined as the PGA [g] vs. the positive and negative direction displacement envelopes of the ridge relative to the base [mm] for each test

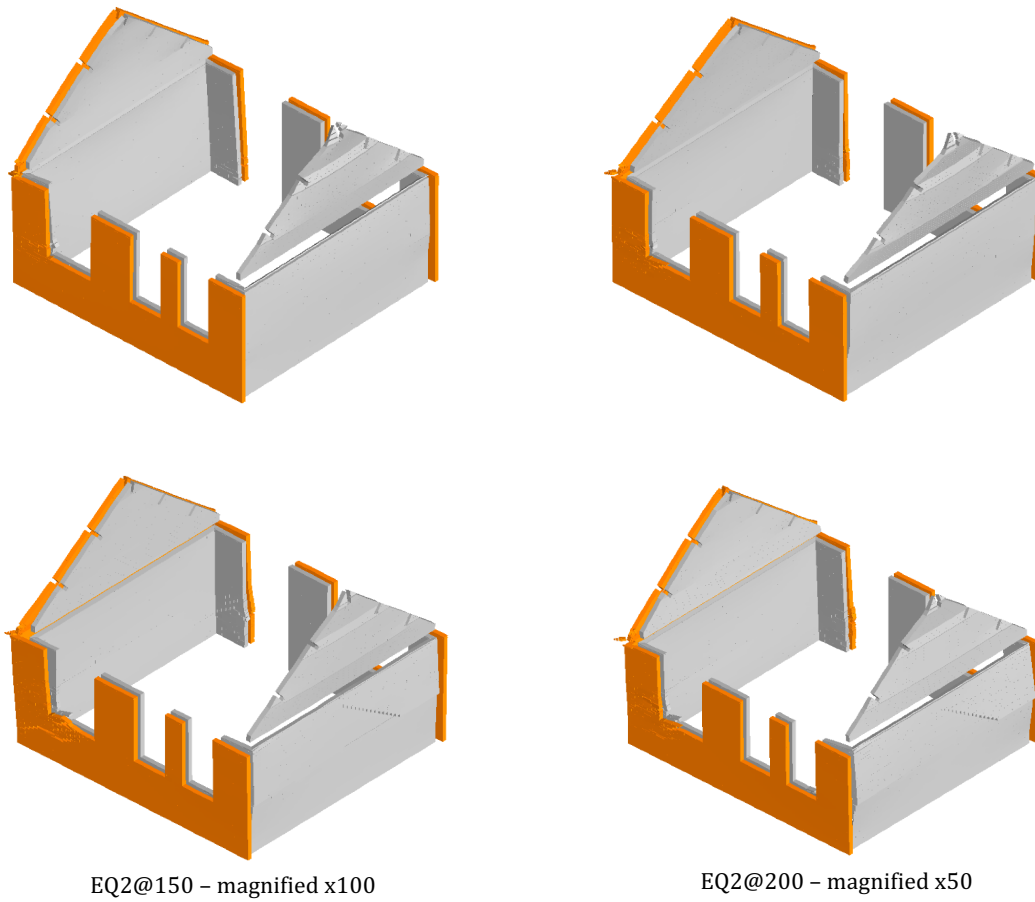
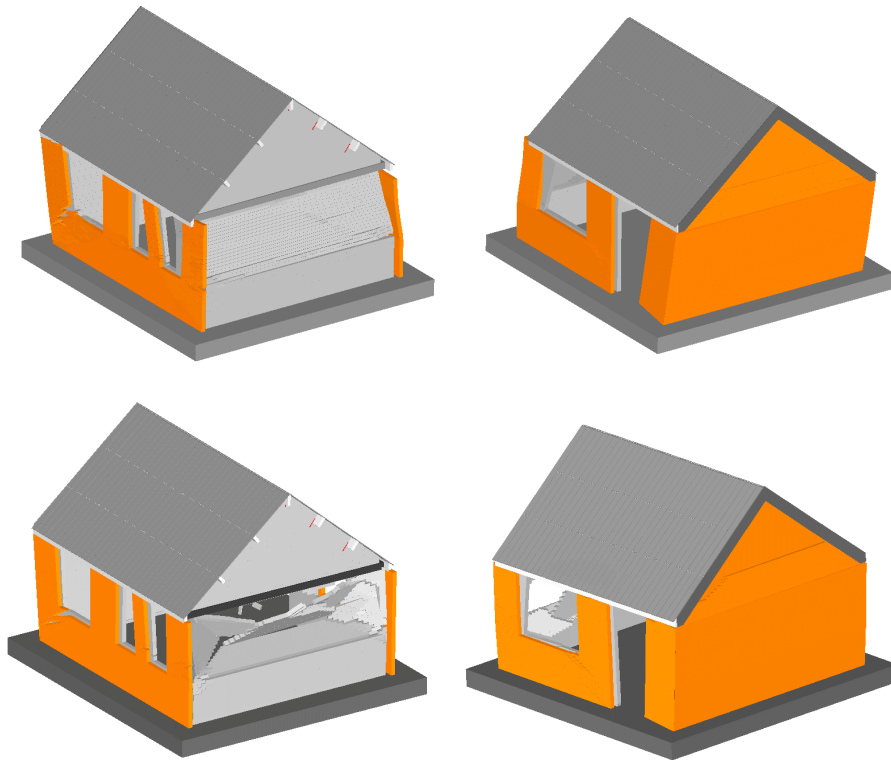


Figure 19 Deflected shapes at maximum excursion prior to collapse

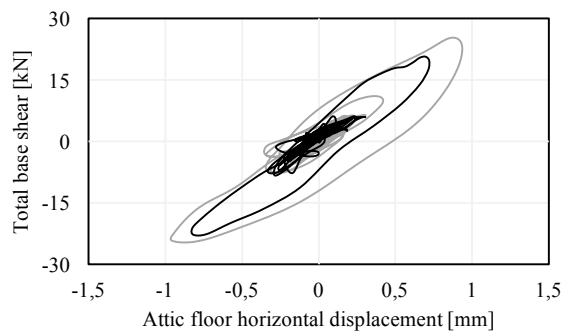


EQ2@300 – magnified x2

Figure 20 Out-of-plane collapse of the CS party wall

4.4 Floor hysteresis

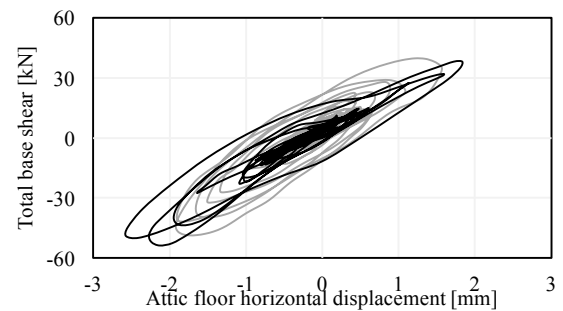
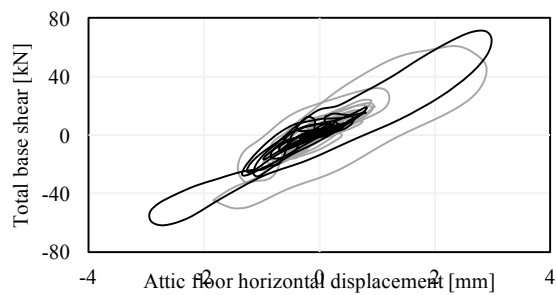
Floor hysteresis is defined as the total “base” shear [kN] vs. attic floor horizontal displacement relative to the base [mm]. Grey is experimental and black is numerical.

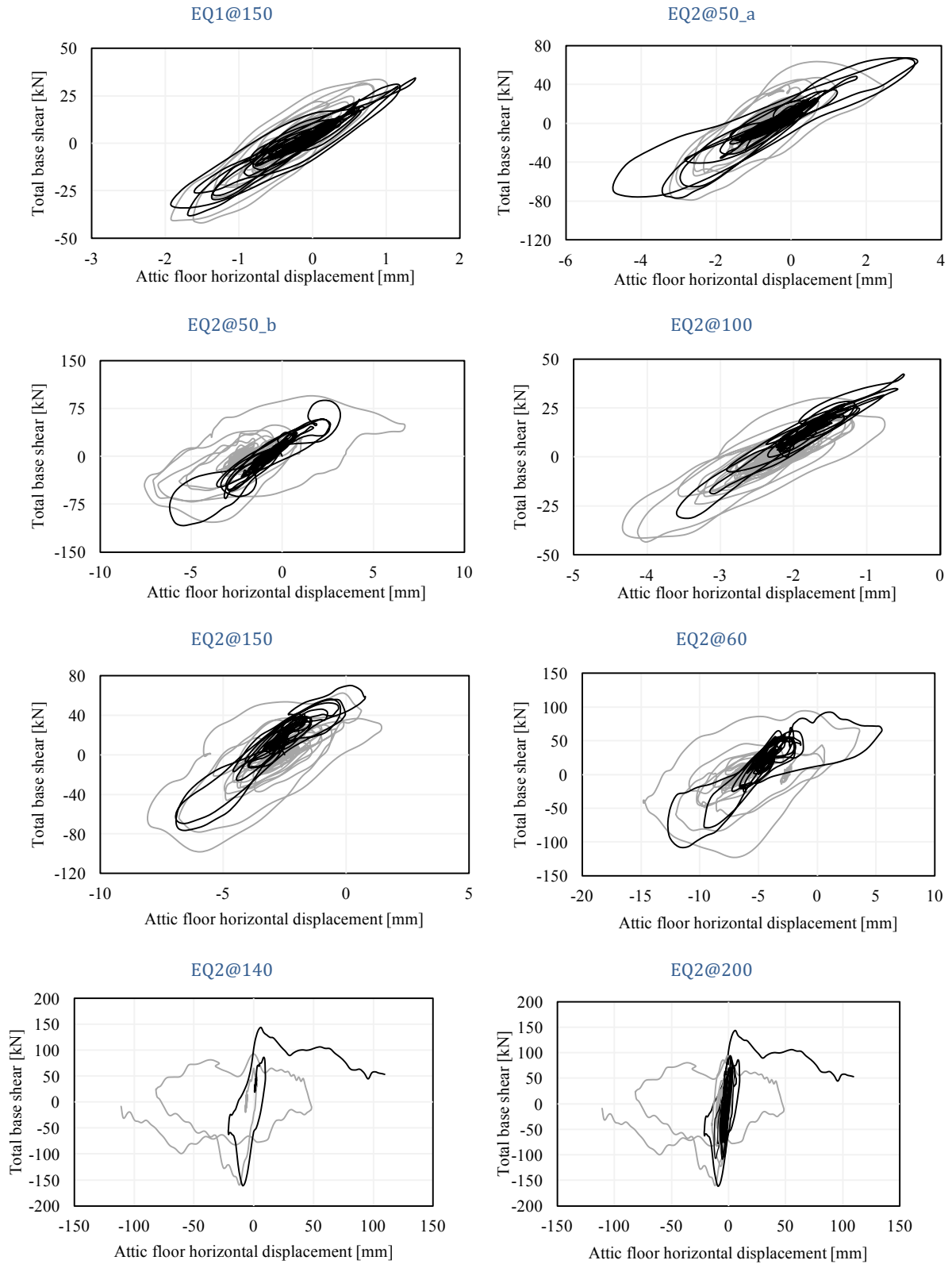


EQ1@50



EQ1@100



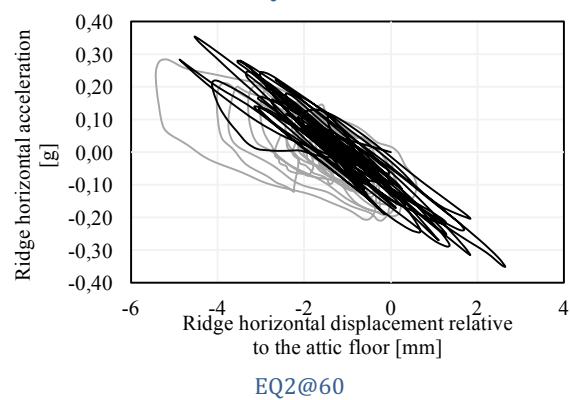
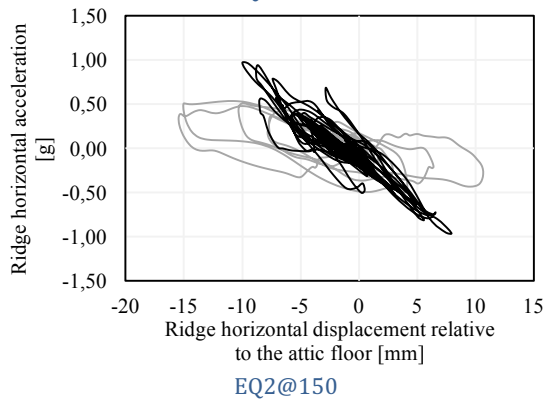
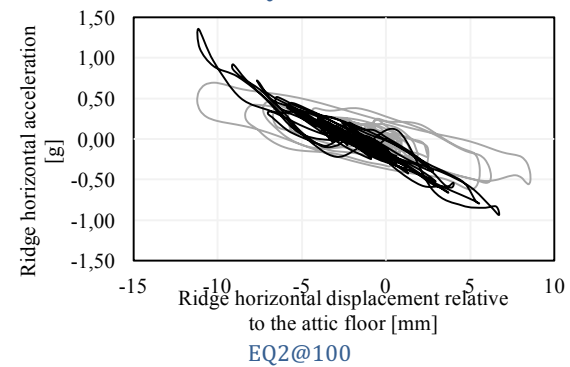
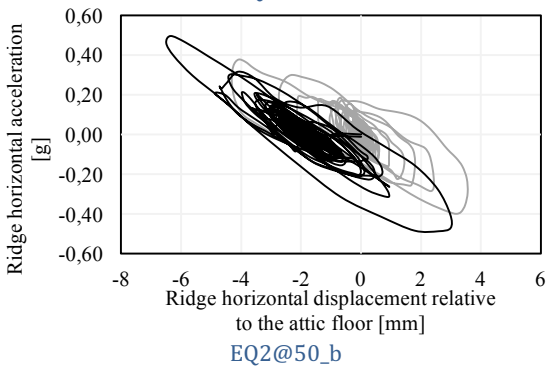
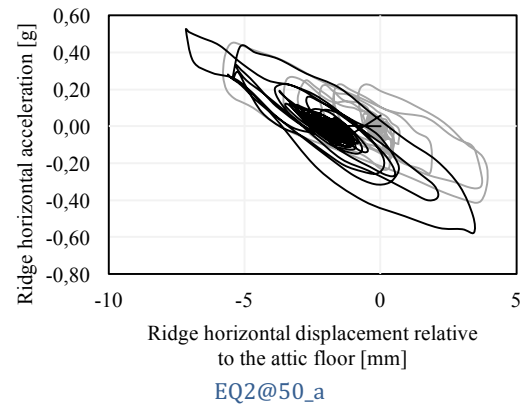
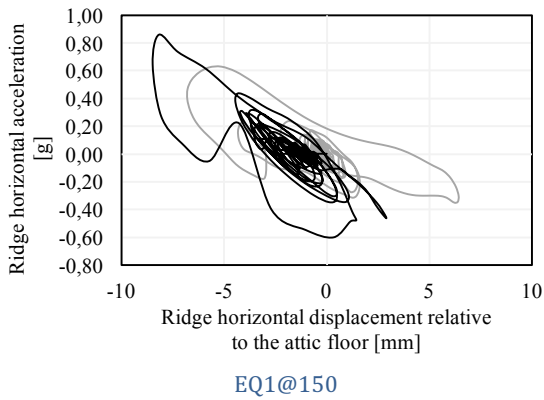
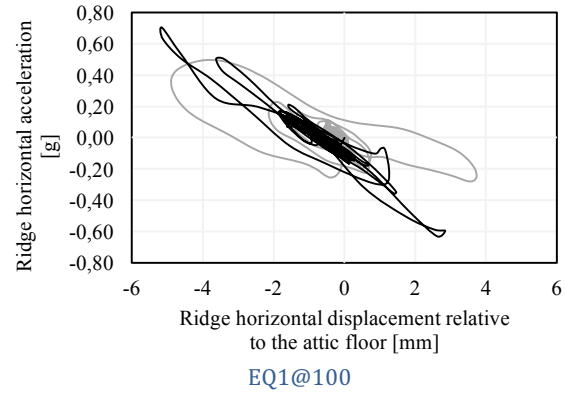
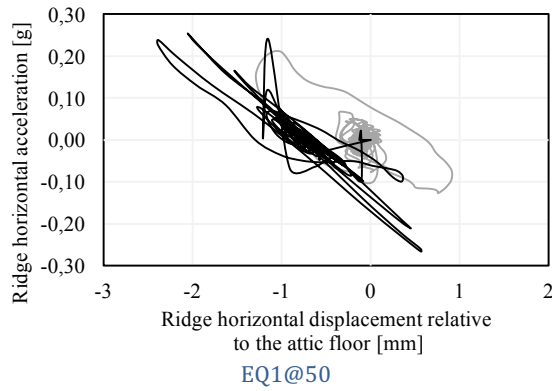


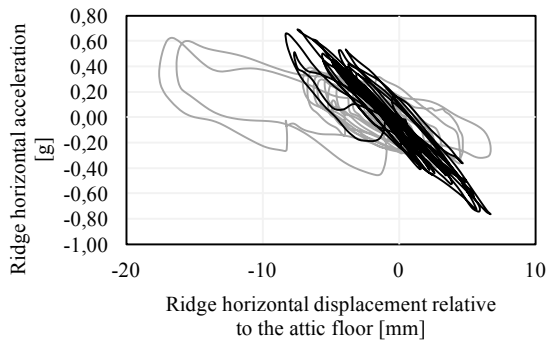
EQ2@300 - collapse

full-cycles hysteresis

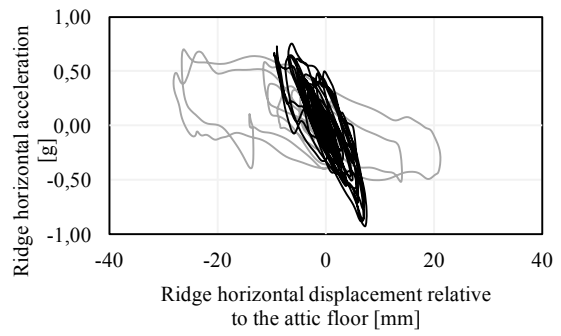
4.5 Roof acceleration hysteresis

Roof acceleration hysteresis is defined as the ridge horizontal acceleration [g] vs. ridge horizontal displacement relative to the attic floor horizontal displacement [mm]. Grey is experimental and black is numerical.

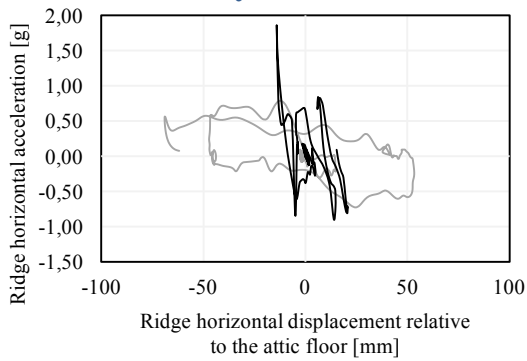




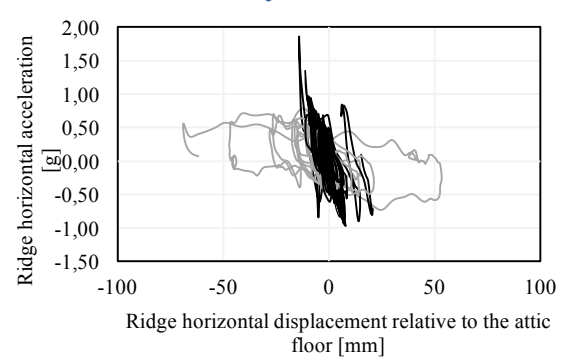
EQ2@140



EQ2@200



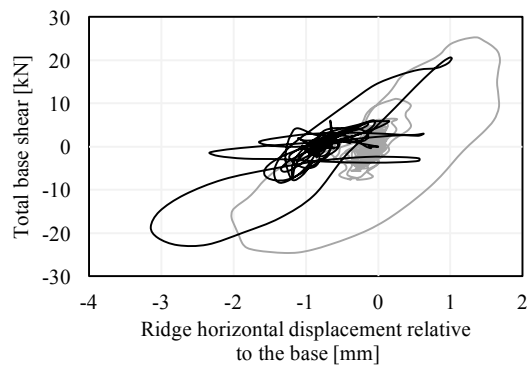
EQ2@300 - collapse



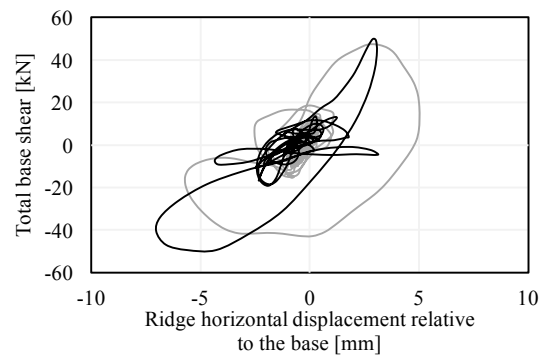
full-cycles hysteresis

4.6 Global hysteresis

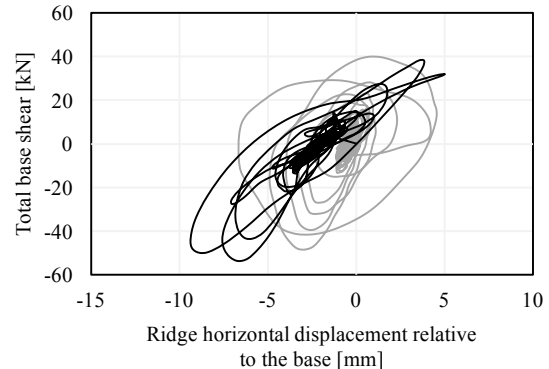
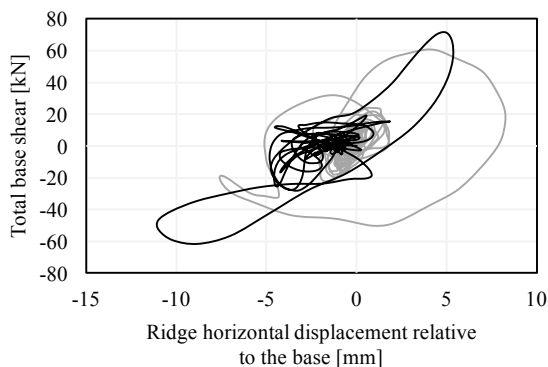
Global hysteresis is the total “base” shear [kN] vs. ridge hor. displacement relative to the base [mm]. Grey is experimental and black is numerical.



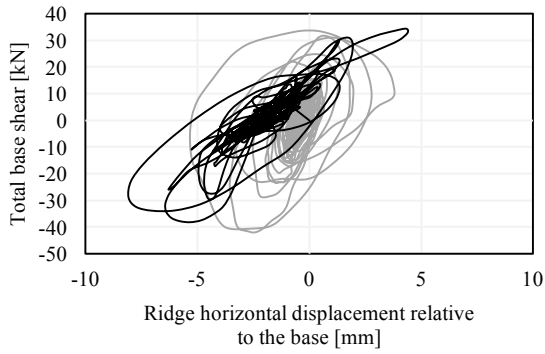
EQ1@50



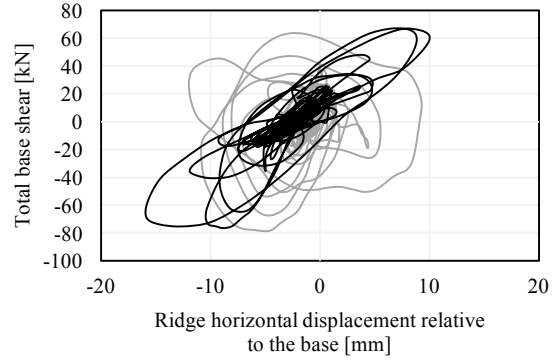
EQ1@100



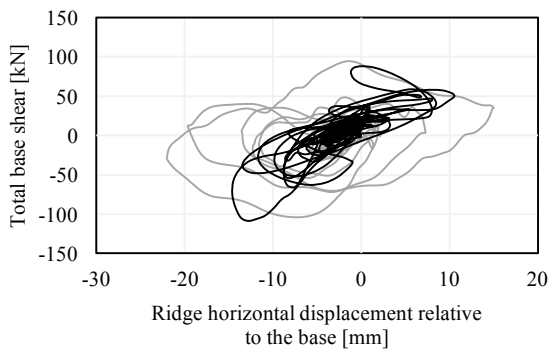
EQ1@150



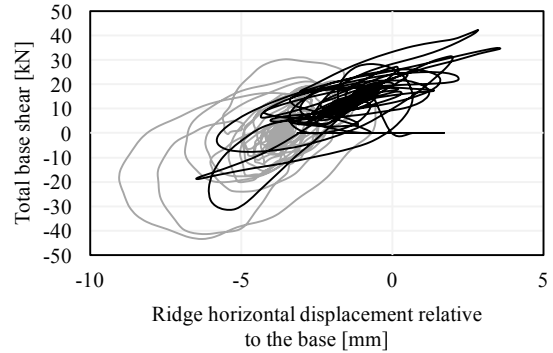
EQ2@50_a



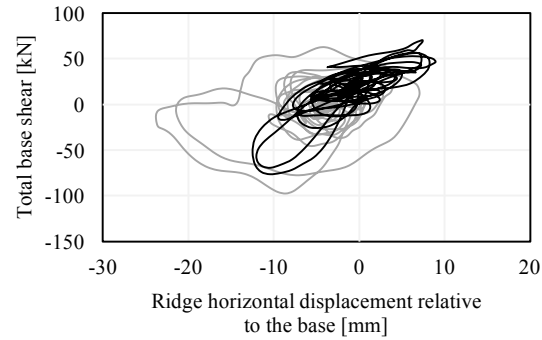
EQ2@50_b



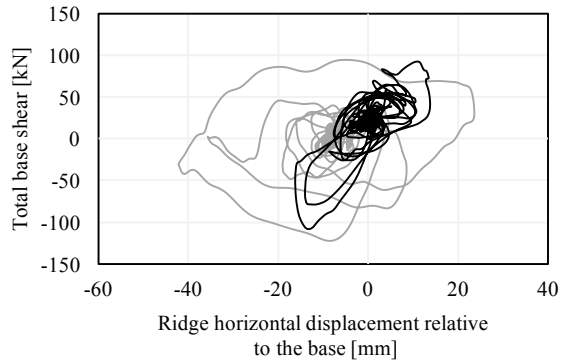
EQ2@100



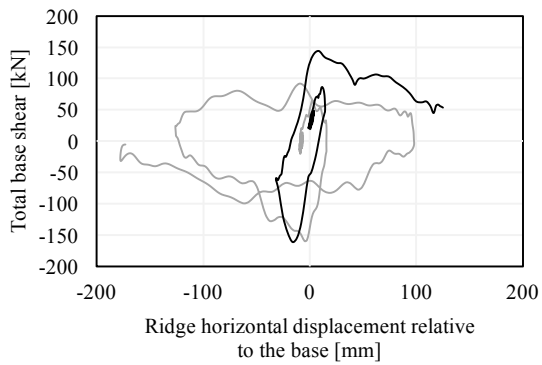
EQ2@150



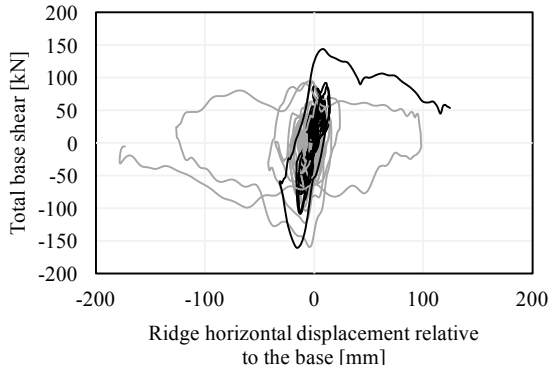
EQ2@60



EQ2@140



EQ2@200



EQ2@300 - collapse

full-cycles hysteresis

4.7 Crack patterns and collapse mechanism

The final damage predictions for each wall (both CS and CL masonry elements) are compared in this sub-Section with their experimental counterpart (varied magnification).

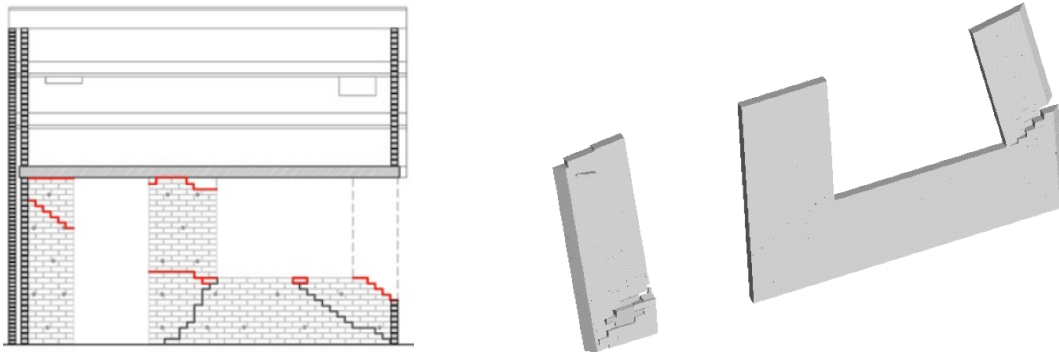


Figure 21 EQ2@300 _ Experimental (left) and numerical (right) damage plot of inner leaf – front wall

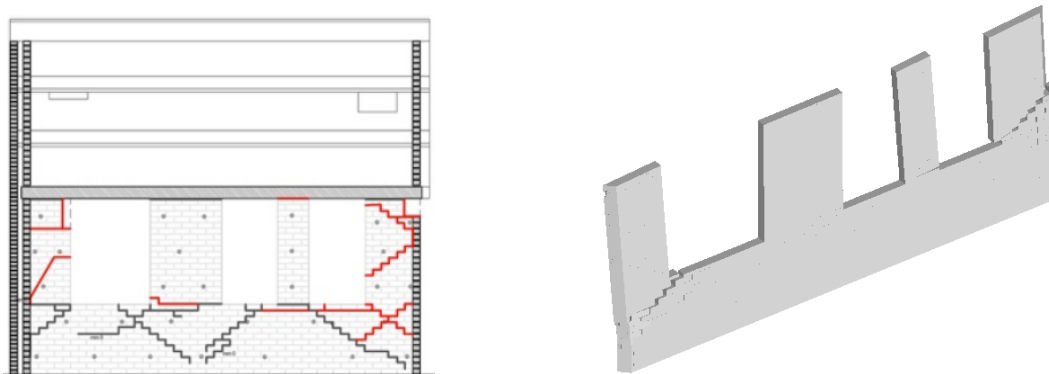


Figure 22 EQ2@300 _ Experimental (left) and numerical (right) damage plot of inner leaf – back wall

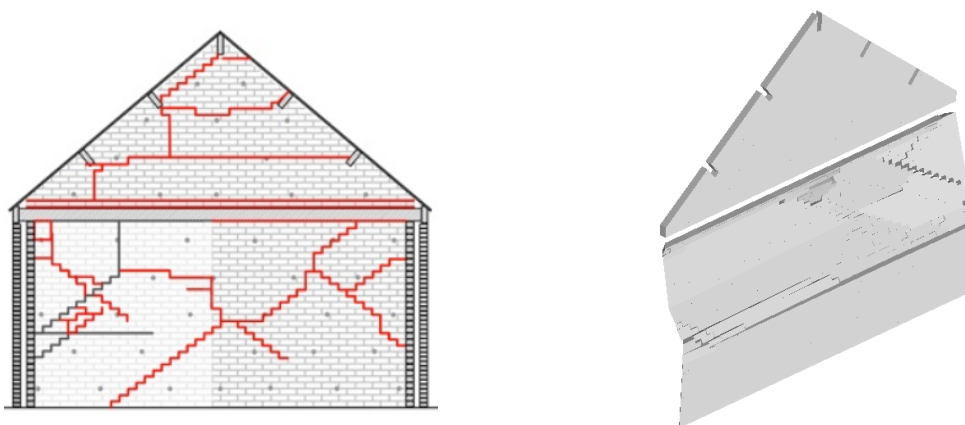


Figure 23 EQ2@300 _ Experimental (left) and numerical (right) damage plot of inner leaf – end wall

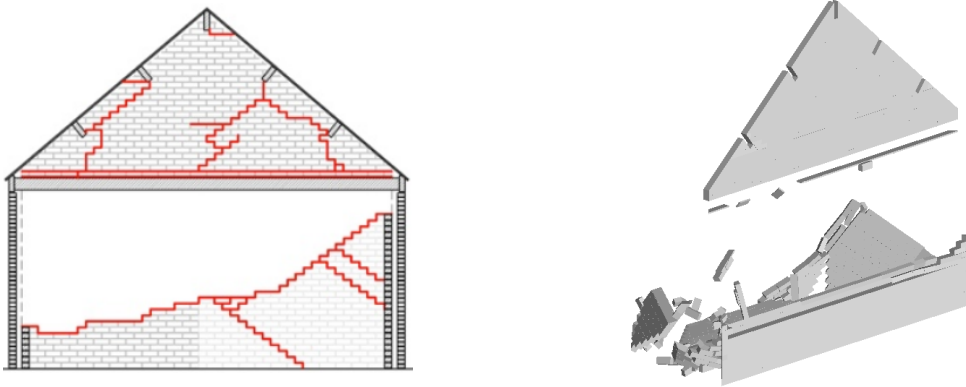


Figure 24 EQ2@300 _ Experimental (left) and numerical (right) damage plot of inner leaf - party wall

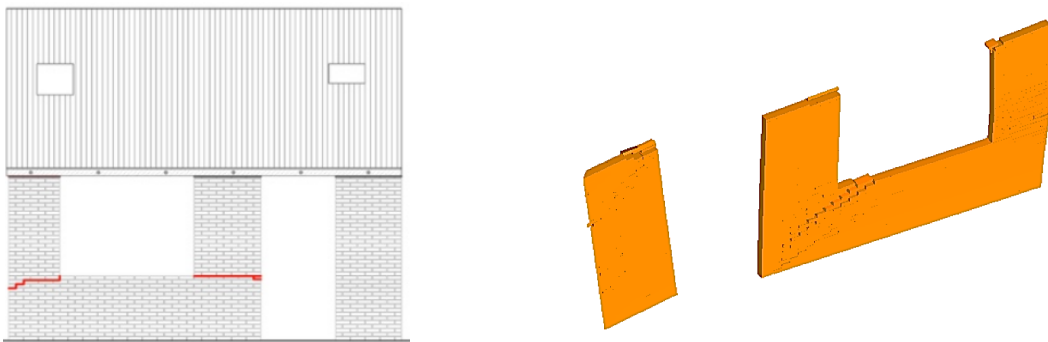


Figure 25 EQ2@300 _ Experimental (left) and numerical (right) damage plot of outer leaf - front wall

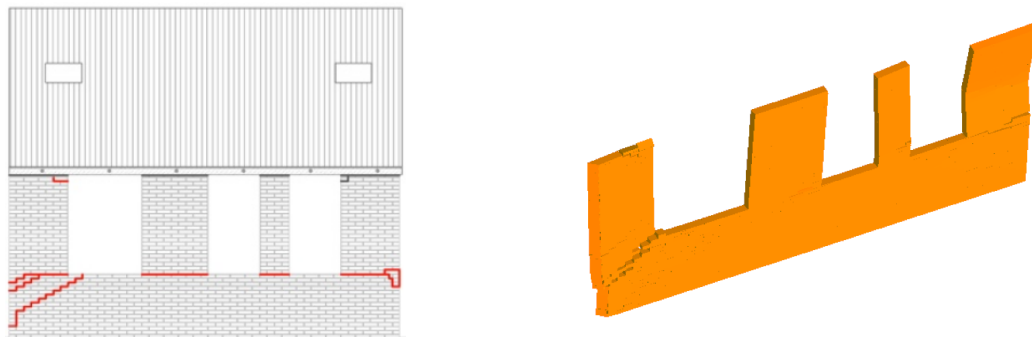


Figure 26 EQ2@300 _ Experimental (left) and numerical (right) damage plot of outer leaf - back wall

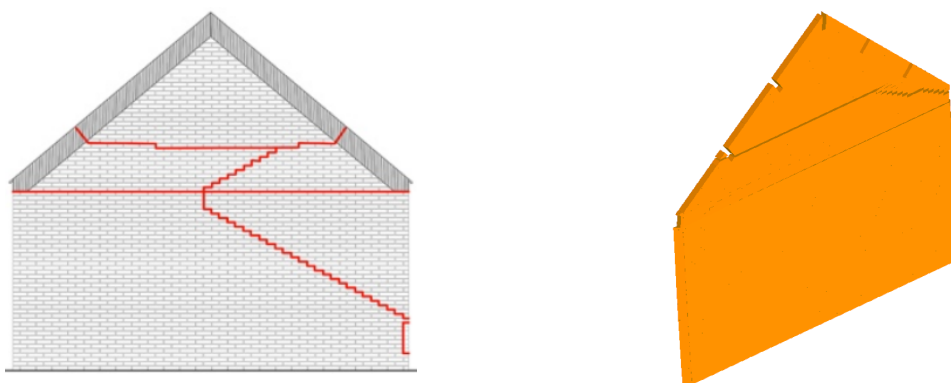


Figure 27 EQ2@300 _ Experimental (left) and numerical (right) damage plot of outer leaf - end wall

Finally, and recapping the main information reported in this Section, it is recalled that the numerical model showed an out-of-plane collapse of the CS party wall during EQ2@300, matching its experimental counterpart. Moreover, it is interesting to note also that, as reported below, the numerical model successfully predicted the RC slab uplift and thus the loss of contact between RC slab and CS party wall (which resulted in the alteration of the initial boundary conditions of the wall). Since this phenomenon was not expected, the vertical displacement of the RC slab was not recorded by the laboratory instrumentation. However, the numerical prediction of 30 mm reported in Figure 28 seems to be reasonable.

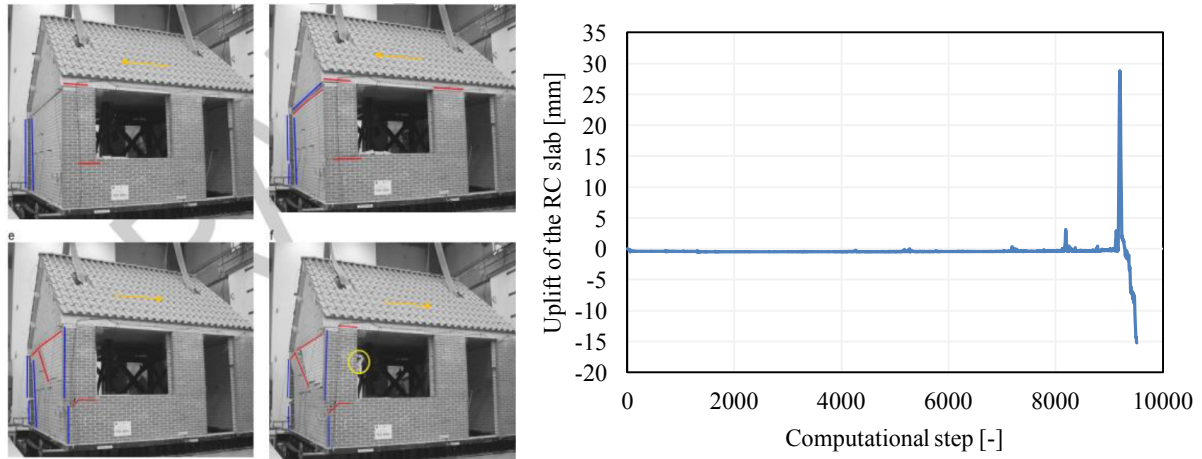


Figure 28 Experimental failure mechanisms and numerical RC slab uplift

5 Closing Remarks

This modelling exercise confirmed the capability of the Applied Element Method in adequately capturing the seismic response of URM buildings, given that the model did reproduce the overall structural response and the partial collapse of the specimen.

Of non-negligible importance is also the fact that, as reported in the tables above, in most cases the modelling properties adopted for the post-test calibrated model coincide with the experimental ones, and no significant adjustments had to be introduced. This is further reassuring for when this modelling approach is employed in contexts where no test data is available.

Nonetheless, the numerical hysteretic response did exhibit a lower energy dissipation capacity, especially in the final stages of the test series. In addition, the behaviour of the roof structure was not well reproduced by the model, which was stiffer and hence led to lower estimations of roof displacements.

Test results of a subsequent experiment (LNEC-BUILD2), involving the shake-table testing of the roof-gables substructure will certainly prove very useful in better understanding how to adequately model the roofs of this type of structures (be it for what concerns the linear/nonlinear stiffness values to adopt, as well as for the calibration of the timber-to-masonry connection).

For what concerns instead the issue of better capturing the energy dissipation observed in the test specimen, several avenues may be explored in the future, including:

- the possibility of adjusting, in the numerical model, the parameters that control degradation of cohesion and tensile strength (currently this is not possible, in the tool employed for these analyses);
- the feasibility of calibrating the equivalent viscous damping (currently this is not possible, in the tool employed for these analyses);
- meshing the bricks (so far modelled as rigid units), so that the energy dissipation associated to their deformation (in particular of CS bricks), cracking, splitting and crushing may be taken into account.

References

- Arup (2017) "LNEC-BUILD-1: Modelling Predictions and Analysis Cross Validation," *Report n. 229746_031.0_REP2004*, Amsterdam, The Netherlands.
- ASI (2017) *Extreme Loading for Structures v5*, Applied Science International LLC., Durham (NC), USA.
- Brooks J.J., Baker A. (1998) "Modulus of elasticity of masonry" *Masonry International*, Vol. 12, No. 2, pp. 58–63.
- Ciesielski R. (1999) "The dynamic module of elasticity of brick walls," *Proceedings of the Conference of the Committee of Civil Engineering PZITB*, Lublin, Poland.
- Graziotti F., Tomassetti U., Rossi A., Kallioras S., Mandirola M., Cenja E., Penna A., Magenes G. (2015) "Experimental campaign on cavity-wall systems representative of the Groningen building stock," *Report n. EUC318/2015U*, European Centre for Training and Research in Earthquake Engineering (EUCENTRE), Pavia, Italy. Available from URL: <http://www.eucentre.it/nam-project>
- ICBO (1991) *Uniform Building Code*, International Conference of Building Officials, USA.
- Kim J.J., Reda Taha M. (2014) "Experimental and numerical evaluation of direct tension test for cylindrical concrete specimens," *Advances in Civil Engineering*, Vol. 2014, pp. 1-8.
- Malomo (2018) "Scrutinising the applicability of the Applied Element Modelling in the modelling of URM structures subjected to earthquake loading," *PhD Thesis*, University of Pavia, Italy. To be Submitted.
- Matysek P., Zbigniew J. (1996) "Analysis of factors affecting the modulus of elasticity of the walls," *Proceedings of the Conference of the Committee of Civil Engineering PZITB*, Lublin, Poland.
- Meguro K., Tagel-Din H. (2000) "Applied Element Method for structural analysis: Theory and application for linear materials," *JSCIE International Journal of Structural Engineering and Earthquake Engineering*, Vol. 17, No. 1, pp. 21–35.
- Meguro K., Tagel-Din H. (2001) "Applied Element simulation of RC Structures under cyclic loading," *ASCE Journal of Structural Engineering*, Vol. 127, No. 11, pp. 1295-1305.
- Meguro K., Tagel-Din H. (2002) "Applied Element Method used for large displacement structure analysis," *Journal of Natural Disaster Science*, Vol. 24, No. 2, pp. 65-82.
- Mosayk (2016) "Using the Applied Element Method to model URM walls subjected to in-plane cyclic shear-compression," Pavia, Italy.
- Tomassetti U., Correia A.A., Graziotti F., Marques A.I., Mandirola M., Candeias P.X. (2017a) "Collapse shaking table test on a URM cavity wall structure representative of a Dutch terraced house," European Centre for Training and Research in Earthquake Engineering (EUCENTRE), Pavia, Italy. Available from URL: <http://www.eucentre.it/nam-project>
- Tomassetti U., Kallioras S., Graziotti F., Correia A. (2017b) "Final report on the construction of the building prototype at the LNEC laboratory," European Centre for Training and Research in Earthquake Engineering (EUCENTRE), Pavia, Italy.

Appendix A – further details on URM model building in ELS

This Appendix is common to a series of reports by Mosayk (2017a, 2017b, 2017c) concerning the modelling of the shake-table testing of a number of URM full-scale specimens (EUC-BUILD1, EUC-BUILD2, LNEC-BUILD1 and LNEC-BUILD2), and aims at providing further details on the modelling of:

- Contact surfaces between elements (mortared or nailed)
- Timber planks (of slabs and roofs)
- Connectors, ties and steel anchors

In addition, the procedure to derive mortar elastic properties by means of homogenisation formulae is also reported.

A.1 AEM modelling of contact surfaces between elements

According to the AEM, the connection between rigid bodies is assured by interface springs. Each contact surface, indeed, is characterised by a user-defined number of springs in which both the material properties and the damping of the system are lumped.

The analysis accuracy is directly proportional to the number of springs as well as the mesh discretisation (i.e. the number of rigid bodies constituting the assembly). In most cases the default value of 25 springs per contact surface is sufficient to represent adequately the actual behaviour of a given structural elements both in static and dynamic range. However, when the numerical model requires a refined discretisation (i.e. a larger number of elements), then if the contact surface is sufficiently small, the amount of interface springs can be reduced consistently, so as to reduce the computation burden. In the analyses presented in this report, indeed, 9 springs per contact surface (of the discretised elements) were employed, given that this proved to constitute a good compromise between accuracy and computational demand.

As depicted in Figure A.1, the springs are located at specific contact points and distributed uniformly along the contact surfaces, representing the stress/strain state of a given volume DV (or DA in 2D), as well as the contact stiffness. This modelling approach thus readily allows assigning equivalent mechanical properties to the contacts in order to describe the actual behaviour of a wide range of connections between different elements (e.g. nailed, welded or interlocking connections).

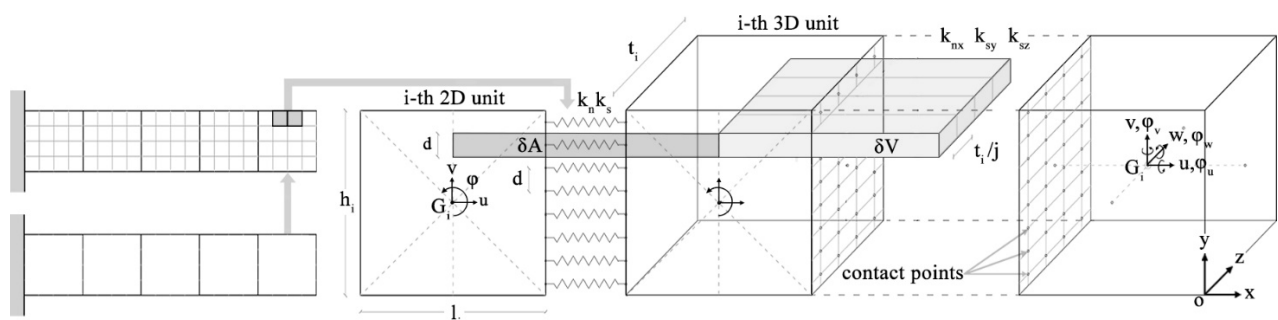


Figure A.1 Multi-scale discretization of both 2D and 3D rigid body assembly

In Figure A.2, below, the different types of contact connections considered in this modelling endeavour (which, it is reiterated, concerned the modelling of the shake-table testing of the four URM full-scale specimens listed above, not all of which are described in this one report) are shown.

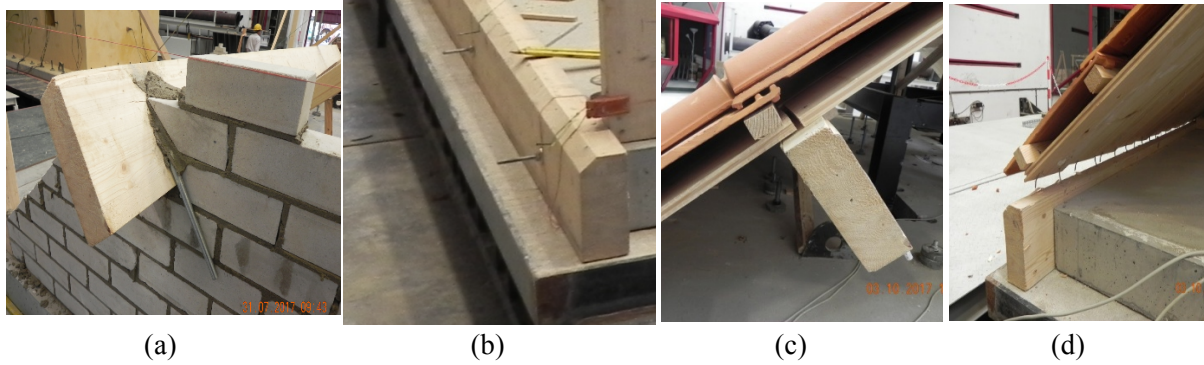


Figure A.2 L-shaped anchors (a), RC slab/beam connection (b), pure frictional contact between walls and planks (c) and nailed connections between boards and ridge/timber plate (d) (Correia et al., 2017)

A.1.1 Nailed connections between beam and plank elements

The mechanical connection between wooden boards and beams in traditional flexible diaphragms, is often provided by one or more steel nails distributed along the contact surface (Brignola et al., 2008) as reported in Figure A.3 below.

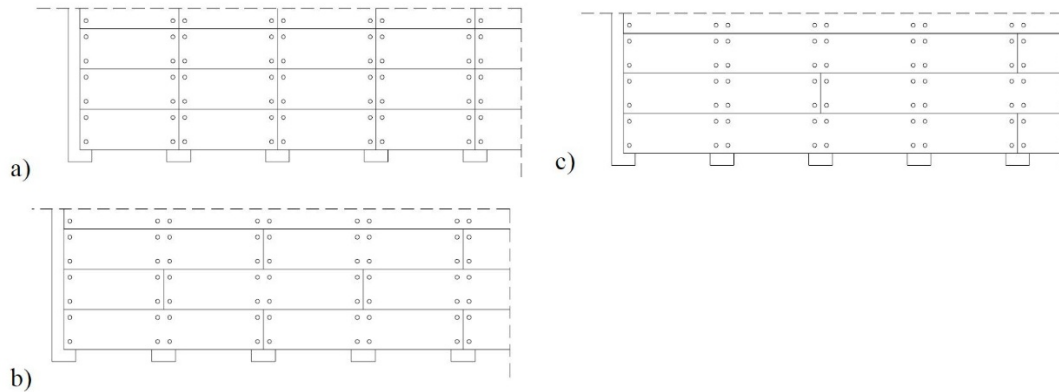


Figure A.3 Types of common nailed connections between beams and boards (Brignola et al., 2008)

The stiffness related to these interfaces are calibrated from the force-slip behaviour of the nail ($k_{ser} = F'/d'$), assuring the actual shear deformability to the connection. According to Eurocode 5 (2004), the slip modulus of a nail with diameter d' can be evaluated by means of Eq. (A.1) below, considering the simplified elastic-perfectly plastic response depicted in Figure A.4. Thus, considering a contact area A_c between board and beam, the following equivalent shear modulus Geq_{nails} , reported in Eq. (A.2) can be introduced and subsequently assigned to the related interface, where L represents the distance from the centroids of elements.

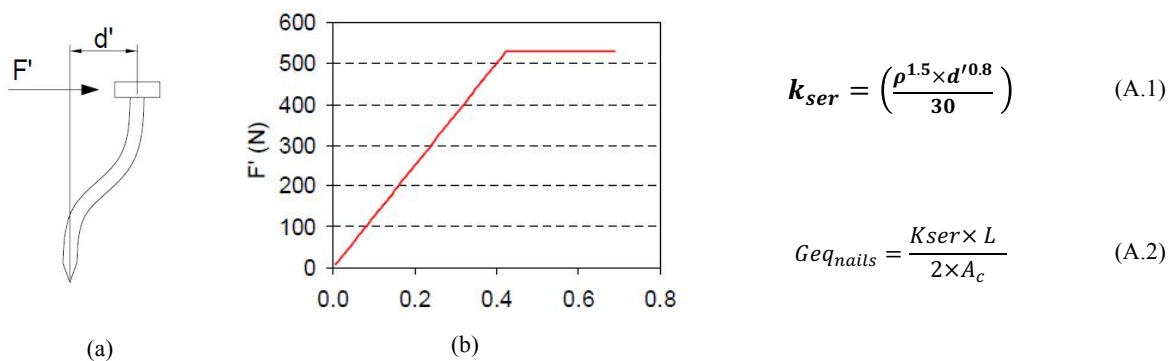


Figure A.4 Nail slip behaviour (a), and its force-displacement bilinear response (b) (Brignola et al., 2008)

With the aim of investigating the numerical response of this type of connection, several simplified models, of the type illustrated below in Figure A.5, were elaborated. In Table A.1 the main equivalent modelling parameters concerning the simplified model (compatible with the roof structure of both EUC-BUILD1, LNEC-BUILD1 and LNEC-BUILD2) are reported, whereas the associated force-displacement curve is depicted in Figure A.5(c).

Table A.1 Mechanical properties assigned to the simplified model

Simplified model subjected to pure shear loading conditions			
Material model	Bilinear material	Equivalent yield stress [MPa]	4
Beam height [mm]	220	Number of nails [-]	1
Board thickness [mm]	20	K_{ser} [N/mm]	965
Distance L between centroids [mm]	120	Yield force [N]	576
Area of contact [mm ²]	14400	Yield displacement [mm]	0.77
Nail diameter [mm ²]	4	$E_{eq,nail}$ [MPa]	11
Poisson coefficient [-]	0.25	$G_{eq,nail}$ [MPa]	4.4

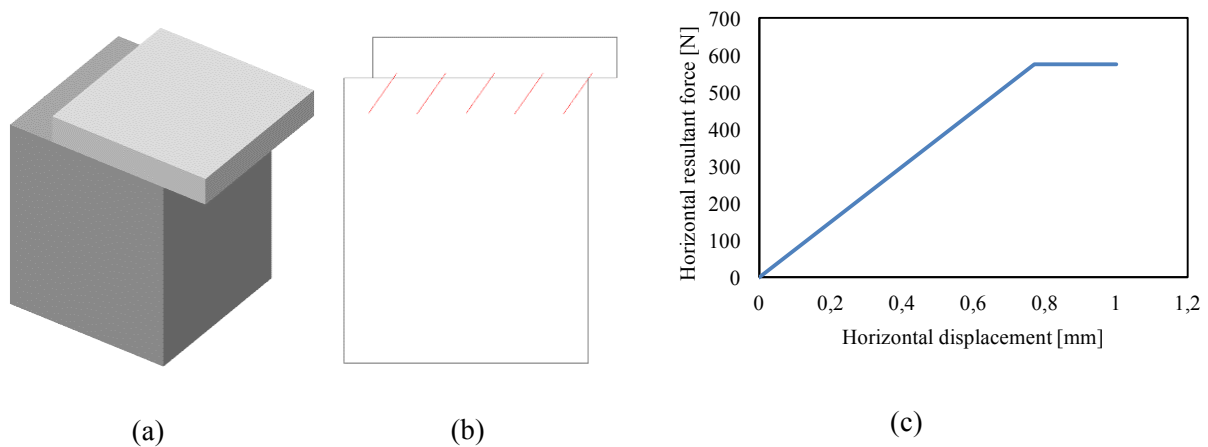


Figure A.5 Screenshot of the model (a), equivalent spring layer representing the nailed connection (b) and force-displacement plot (c)

In the abovementioned model, the base (beam) was fully fixed, whereas the upper element (plank) was free to move in the horizontal direction only. Hence, the interface springs were subjected to pure shear. With a view to account for the rotational deformability as well, the elastic modulus of the nail was inferred by multiplying $G_{eq,nail}$ by a factor of 2.5, yielding the typical constitutive equation for isotropic materials (Lekhnitskii, 1963).

However, further improvements related to the latter aspects are needed. Since the yield stress can be reached both in tension and in pure shear, the preliminary modelling results obtained for LNEC-BUILD1 using this methods prior the shake-table test, for instance, have shown that an early tensile failure of the connection (reached due to the increase in the rotation demand due to the relative displacement of adjacent boards) might occur.

Hence, small variations of this approach have been employed and applied for the subsequent models. For EUC-BUILD1, EUC-BUILD2, LNEC-BUILD1 and LNEC-BUILD2 (post-test refined simulations), indeed, the equivalent yield stress was increased consistently to avoid the early rotational failure of the beam-plank interface, as reported in Table A.2. This effectively rendered the updated contact surface as featuring an equivalent elastic interface, limited by the actual shear stiffness of the nail.

Table A.2 Mechanical properties of the nailed connection for EUC-BUILD2, LNEC-BUILD1 and LNEC-BUILD2

LNEC-BUILD1 (blind prediction model)			
Material model	Bilinear material	Equivalent yield stress [MPa]	4
Beam height [mm]	220	Number of nails [-]	2
Board thickness [mm]	20	K_{ser} [N/mm]	965
Distance L between centroids [mm]	120	Yield force [N]	---
Area of contact [mm ²]	14400	Yield displacement [mm]	---
Nail diameter [mm ²]	4	$E_{eq,nail}$ [MPa]	22
Poisson coefficient [-]	0.25	$G_{eq,nail}$ [MPa]	8.8
EUC-BUILD1, LNEC-BUILD1, LNEC-BUILD2 (post-test refined models)			
Material model	Bilinear material	Equivalent yield stress [MPa]	360
Beam height [mm]	220	Number of nails [-]	2
Board thickness [mm]	20	K_{ser} [N/mm]	965
Distance L between centroids [mm]	120	Yield force [N]	---
Area of contact [mm ²]	14400	Yield displacement [mm]	---
Nail diameter [mm ²]	4	$E_{eq,nail}$ [MPa]	22
Poisson coefficient [-]	0.25	$G_{eq,nail}$ [MPa]	8.8
EUC-BUILD2			
Material model	Bilinear material	Equivalent yield stress [MPa]	360
Beam height [mm]	180	Number of nails [-]	40 ¹
Board thickness [mm]	24	K_{ser} [N/mm]	965
Distance L between centroids [mm]	102	Yield force [N]	---
Area of contact [mm ²]	410000 ¹	Yield displacement [mm]	---
Nail diameter [mm ²]	4	$E_{eq,nail}$ [MPa]	13
Poisson coefficient [-]	0.25	$G_{eq,nail}$ [MPa]	5

¹ referred to the average contact area between a single transverse frame and the equivalent membrane element

A.1.2 Definition of “weak” and “cracked” mortar spring interfaces

In some cases (i.e. the modelling of EUC-BUILD1 and LNEC-BUILD1, post-test refined model) the connection between the lateral timber beam of the wooden roof structure, the RC slab and the URM cavity-wall system was characterised by peculiar mechanical properties. Indeed, the connection between the RC slab and the lateral timber beam of both EUC-BUILD1 and LNEC-BUILD1 consisted in a series of threaded bars (Graziotti et al., 2015), with the RC slab being then bonded to the transverse CS walls, while the beam is connected by means of a mortar layer to the CL brick masonry transverse walls.

Noteworthy, and also as gathered from Figure below, for both the specimens the gap between the RC slab and the longitudinal walls was filled after the temporary supports removal (i.e. after RC slab deflection); since the connection between these elements was provided only by this mortar layer, a “weak” spring interface was adopted, with a very low flexural and shear stiffness.

Further, in the case of LNEC-BUILD1, with aim to take into account the damage occurred at the interface between the RC slab and the lateral during transportation phases (Tomassetti et al., 2017), a “cracked” mortar spring interface has been introduced. This layer has almost zero flexural and shear stiffness, zero tensile and shear strength, and a compressive strength equal to the one of the brick.



Figure A.6 Constructional details of the gap between CL walls/timber beam (a) and CS walls/RC slab (b) (Graziotti et al., 2015)

A.2 Numerical modelling of plank elements

The overall diaphragm flexibility can be evaluated by analysing the contribution to the in-plane deformation of the timber floor separately, as suggested by Brignola et al. (2008). In this sense, three different deformability contributions are distinguished: the flexural deformation of the single board, shear deformation of the single board and the rigid rotation of the board due to nails slip (see Figure A.7).

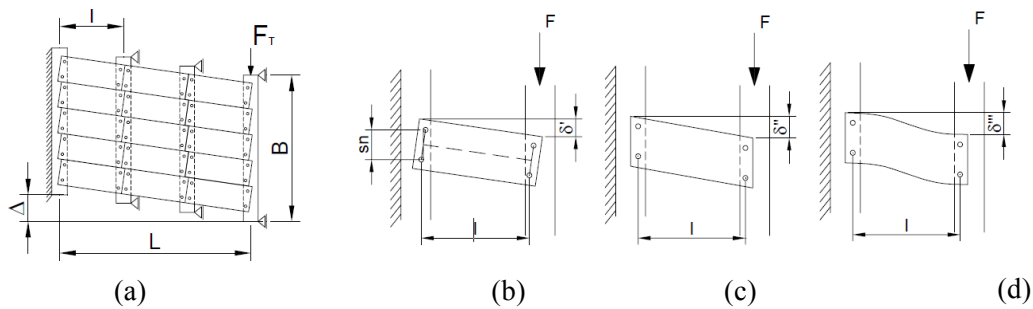


Figure A.7 Deformability contributions of a given flexible diaphragm (Brignola et al., 2008)

Thus, it is possible to define an equivalent shear modulus that combines the three contributions of flexibility according to Eq. (A.3), where X is the shear factor, G shear modulus of planks, E flexural modulus parallel to grain of planks, A board section, I moment of inertia of plank section and s_n is the wheelbase between beams. Moreover, this result obtained for one board can be extended to the whole diaphragm when the wood planks are interrupted at each beams, as noted by Brignola et al. (2008).

$$Geq_{plank} = \left(\frac{X}{A}\right) \left(\frac{l}{k_{ser} s_n^2} + \frac{X}{GA} + \frac{L}{12EI}\right)^{-1} \quad (A.3)$$

However, since the deformability of nails is already accounted by the spring interface described in the previous sub-section, Eq. (A.4) can be simplified as follows:

$$Geq_{plank} = \left(\frac{X}{A}\right) \left(\frac{X}{GA} + \frac{L}{12EI}\right)^{-1} \quad (A.4)$$

Two main modelling strategies have been employed for modelling the roof structures of the URM full-scale specimens mentioned above, due to different construction details. Indeed, the roof of EUC-BUILD1, LNEC-BUILD1 and LNEC-BUILD2 was a relatively simple bearing system,

constituted by longitudinal beams covered by transverse boards and tiles (see Figure A.8). The roof of EUC-BUILD2, instead, was formed by a series of wooden frames supporting the planks and tiles assembly. Furthermore, the gable structure required specific constructional details, as described in the related report (Graziotti et al., 2016).

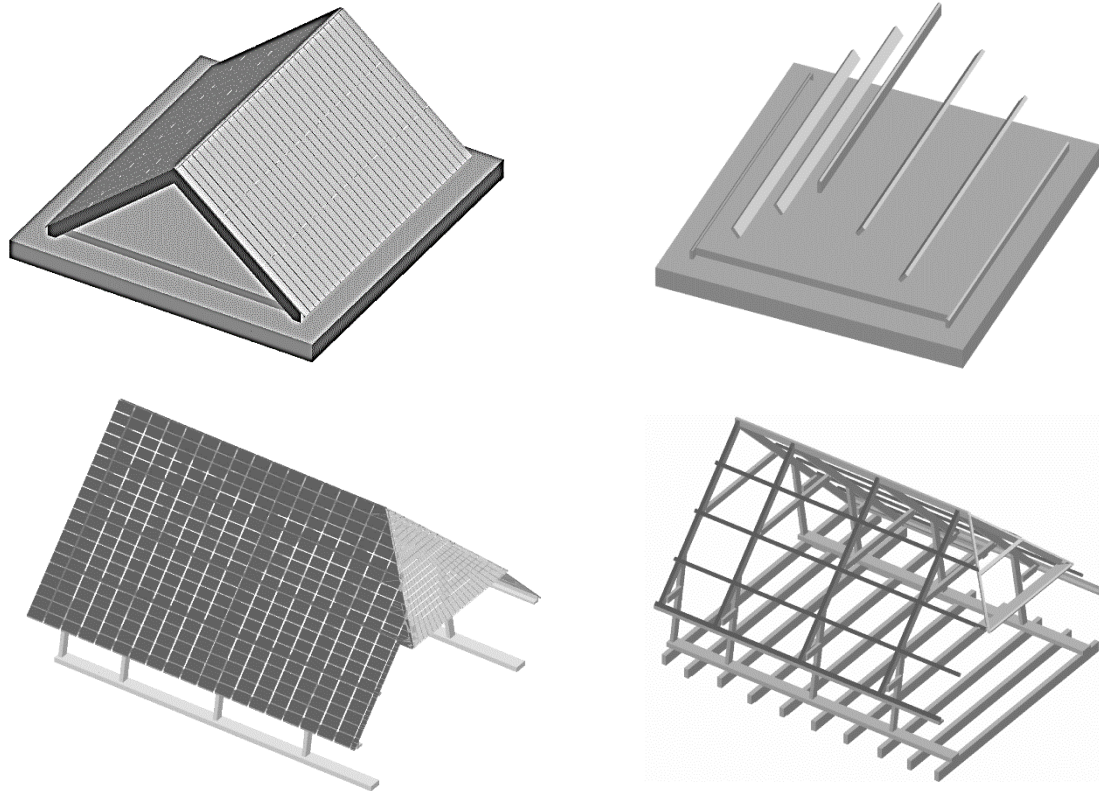


Figure A.8 Roof structure of LNEC-BUILD2 (above) and EUC-BUILD2 (below)

Hence, in case of EUC-BUILD1, LNEC-BUILD1 and LNEC-BUILD2 each plank was modelled separately, resulting in a more accurate numerical response, whereas the planks of EUC-BUILD2 were modelled as an equivalent continuous membrane with the aim of reducing the computational burden and the modelling efforts. The latter approach, as it is clearly observable from the results shown in the corresponding report, still requires further enhancements.

In Table A.3, the main numerical parameters, inferred using Eq. (A.4) and subsequently employed for the modelling of the abovementioned full-scale specimens, are briefly summarised:

Table A.3 Plank material properties employed for the modelling of for EUC-BUILD2, LNEC-BUILD1 and LNEC-BUILD2

LNEC-BUILD1 (blind prediction model)			
Geometrical parameters		Inferred values	
Board thickness	20 mm	Shear factor	1.2
Board width	180 mm	Shear deformation of the single board	8e-07 m/N
Elastic modulus of wood	12000 MPa	Deformability due to rigid rotation of the board	5.18e-0.5 m/N
Shear modulus of wood	750 MPa	Flexural deformation of the single board	4.16e-06 m/N
Board Length	1.8 m	Equivalent shear modulus $G_{eq,plank}$	120.80 MPa
EUC-BUILD1, LNEC-BUILD1, LNEC-BUILD2 (post-test refined models)			
Board thickness	20 mm	Shear factor	1.2
Board width	180 mm	Shear deformation of the single board	8e-07 m/N

Elastic modulus of wood	12000 MPa	Deformability due to rigid rotation of the board	5.18e-05 m/N
Shear modulus of wood	750 MPa	Flexural deformation of the single board	4.16e-06 m/N
Board Length	1.8 m	Equivalent shear modulus $Ge_{q_{plank}}$	120.80 MPa
EUC-BUILD2			
Board thickness	18 mm	Shear factor	1.2
Board width	150 mm	Shear deformation of the single board	2.67e-06 m/N
Elastic modulus of wood	5000 MPa	Deformability due to rigid rotation of the board	7.43e-05 m/N
Shear modulus of wood	333 MPa	Flexural deformation of the single board	2.63e-05 m/N
Board Length	2.0 m	Equivalent shear modulus $Ge_{q_{plank}}$	22.98 MPa

A.3 Connectors, ties and steel anchors elements

The use of metal reinforcements and connectors, such as ties and L-shaped anchors (see Figure A.9), is a relatively common practice in the construction of URM buildings in the Groningen area. These elements, as confirmed also by experimental tests on structural sub-components (Graziotti et al., 2015), strongly affect the behaviour of URM constructions. In Figure A.10 the modelling of the ties elements and the L-shaped steel anchors for EUC-BUILD1 and LNEC-BUILD1 is shown.

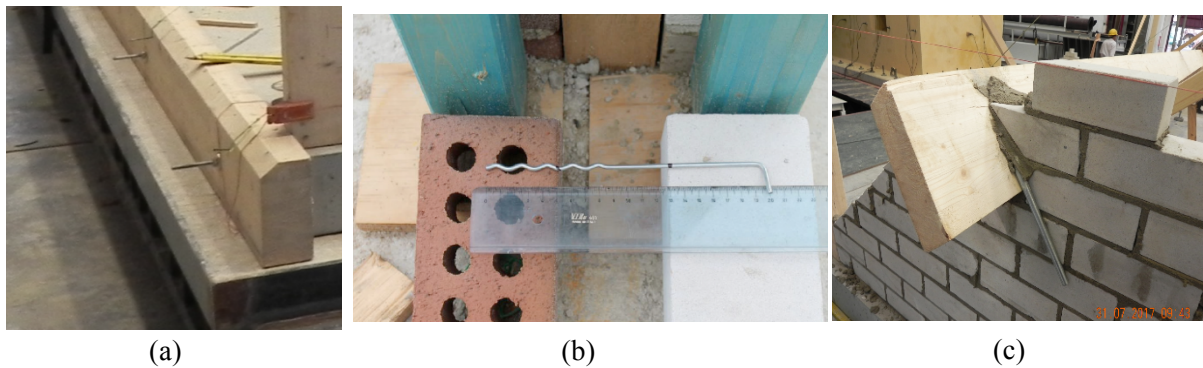


Figure A.9 RC slab/beam connection (a), steel ties (b) and L-shaped anchors (c) (Correia et al., 2017)

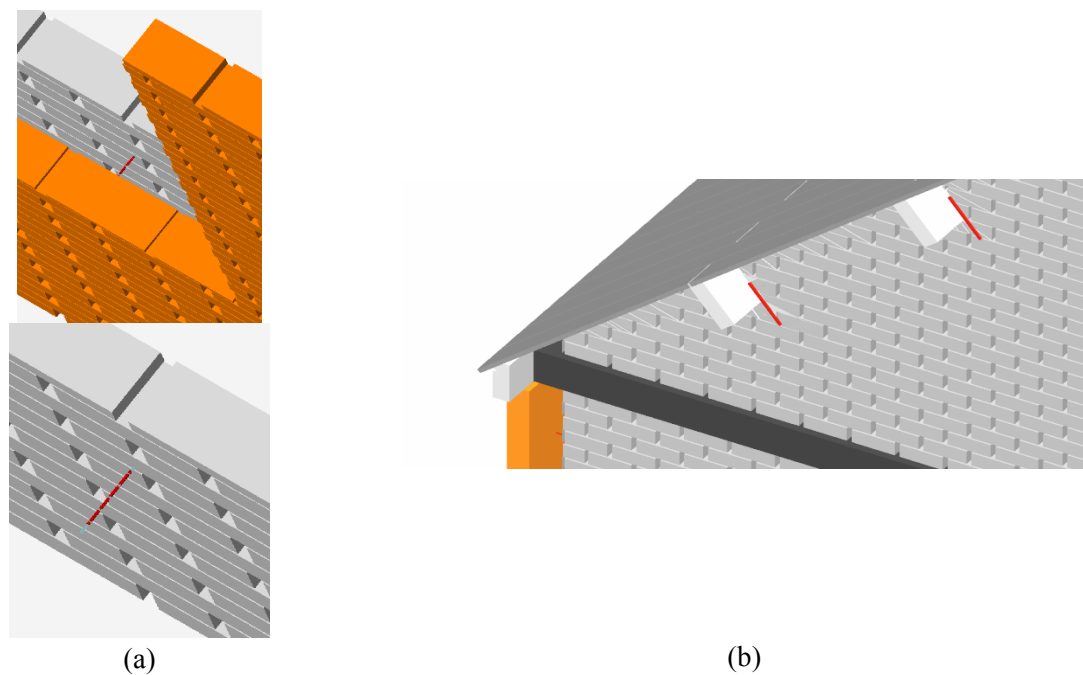


Figure A.10 Nails connections of EUC-BUILD1 (a) and L-shaped anchors of LNEC-BUILD1 (b)

As mentioned above, the connectors between the RC slab and the lateral timber beams were made of threaded bars (diameter of 10 mm). The steel ties connecting the CS to the CL brick masonry walls were instead characterised by a diameter of 3.4 mm, whereas the L-shaped steel anchors (diameter of 15 mm) assured the connection between the timber beam extremities and the gables.

The RC slab/lateral timber beam connector was modelled as an equivalent elastic spring interface, avoiding spurious relative displacement not observed during the tests, whereas both the L-shaped anchors and the ties were modelled by means of three-dimensional beam elements.

In Table A.4, the constitutive models and the most relevant mechanical properties are briefly summarised:

Table A.4 Constitutive models and mechanical properties of metal connectors and anchors

EUC-BUILD1, LNEC-BUILD1, LNEC-BUILD2			
RC slab/lateral timber beams		L-shaped anchors and steel ties	
Material model	Elastic material	Material model	Bilinear material
Element type	Spring interface	Element type	3D girder
Young's modulus [MPa]	10000	Young's modulus [MPa]	210000
Shear modulus [MPa]	400	Shear modulus [MPa]	84000
Friction coefficient [-]	0.4	Friction coefficient [-]	0.8
Separation strain [-]	1e+08	Separation strain [-]	100

A.4 Derivation of mortar Young's modulus from homogenisation formulae

As extensively discussed in Mosayk (2016), since the Young's modulus for both the masonry panels assembly and the bricks are known (from material characterisation tests), the Young's modulus of the mortar can be computed by means of the equations reported in Table A.5, often employed to develop a homogenisation process (i.e. to estimate the Young's modulus of a masonry panel when in knowledge of the Young's moduli of its brick and mortar components).

All four equations described below, where ξ is the ratio of brick's height to the thickness of mortar joint, were used to infer E_{mo} , and then the ensuing average considered for the models. It is noted that when unrealistic values were obtained from a given equation, such values were not considered in computation of the average value.

Furthermore, it is noted that the shear modulus G_{mo} was obtained assuming $G = E/(2(1 + \nu)) = 0.4E$ with $\nu = 0.25$, because no experimental data concerning this specific parameter was available.

Table A.5 Derivation of the Young's modulus of mortar through homogenization criteria

Reference	Homogenisation formulae		Reference	Homogenisation formulae	
Brooks et al. (1998)	$E_{mo} = \left(\frac{-4E_m E_b}{25E_m - 29E_b} \right)$	(A.5)	Matysek et al. (1996)	$E_{mo} = \left(\frac{E_m E_b}{E_b - 1.25\xi(E_m - E_b)} \right)$	(A.6)
Ciesielski (1999)	$E_{mo} = \left(\frac{-E_m E_b}{5E_m - 6E_b} \right)$	(A.7)	ICBO (1991)	$E_{mo} = \left(\frac{E_m E_b}{\xi(E_m - E_b) + E_b} \right)$	(A.8)

In the following Table A.6, the mortar Young's moduli and the mean values subsequently adopted for the modelling of the full-scale URM specimens are reported.

Table A.6 Mortar Young's modulus calculation for each full-scale specimen

LNEC-BUILD1 (blind prediction model)			
CS			
Reference	E_{mo} [MPa]	Reference	E_{mo} [MPa]
Brooks et al. (1998)	895	Matysek et al. (1996)	675
Ciesielski (1999)	1060	ICBO (1991)	1360
Mean value [MPa]			
997			
CL			
Reference	E_{mo} [MPa]	Reference	E_{mo} [MPa]
Brooks et al. (1998)	2927	Matysek et al. (1996)	2927
Ciesielski (1999)	3261	ICBO (1991)	Not reliable
Mean value [MPa]			
3039			
LNEC-BUILD1, LNEC-BUILD2 (post-test refined models)			
CS			
Reference	E_{mo} [MPa]	Reference	E_{mo} [MPa]
Brooks et al. (1998)	4626	Matysek et al. (1996)	3935
Ciesielski (1999)	5059	ICBO (1991)	Not reliable
Mean value [MPa]			
4537			
CL			
Reference	E_{mo} [MPa]	Reference	E_{mo} [MPa]
Brooks et al. (1998)	3184	Matysek et al. (1996)	3184
Ciesielski (1999)	4237	ICBO (1991)	Not reliable
Mean value [MPa]			
3039			
EUC-BUILD1			
CS			
Reference	E_{mo} [MPa]	Reference	E_{mo} [MPa]
Brooks et al. (1998)	4626	Matysek et al. (1996)	3935
Ciesielski (1999)	5059	ICBO (1991)	Not reliable
Mean value [MPa]			
4537			
CL			
Reference	E_{mo} [MPa]	Reference	E_{mo} [MPa]
Brooks et al. (1998)	Not reliable	Matysek et al. (1996)	Not reliable
Ciesielski (1999)	Not reliable	ICBO (1991)	Not reliable
Adopted value [MPa]			
4537 (equal to the one of the CS mortar)			
EUC-BUILD2			
CL			
Reference	E_{mo} [MPa]	Reference	E_{mo} [MPa]
Brooks et al. (1998)	4508	Matysek et al. (1996)	4508
Ciesielski (1999)	4805	ICBO (1991)	Not reliable
Mean value [MPa]			
4607			

A.5 References

- Brignola, A., Podestà, S., Pampanin, S. (2008) "In-plane stiffness of wooden floor" *Proceedings of the New Zealand Society for Earthquake Engineering Conference*, Wellington, New Zealand.
- Eurocode 5, "Design of timber structures", EN 1995-1-1 (2004)
- Graziotti F., Tomassetti U., Rossi A., Kallioras S., Mandirola M., Cenja E., Penna A., Magenes G. (2015) "Experimental campaign on cavity-wall systems representative of the Groningen building stock," *Report n. EUC318/2015U*, European Centre for Training and Research in Earthquake Engineering (EUCENTRE), Pavia, Italy. Available from URL:
- Graziotti F., Tomassetti U., Rossi A., Kallioras S., Mandirola M., Penna A., Magenes G. (2016) "Experimental campaign on a clay URM full-scale specimen representative of the Groningen building stock," *Report n. EUC128/2016U*, European Centre for Training and Research in Earthquake Engineering (EUCENTRE), Pavia, Italy. Available from URL: <http://www.eucentre.it/nam-project>
- Lekhnitskii S.G., Fern P. (1964) "Theory of Elasticity of an Anisotropic Elastic Body," *Physics Today*, Vol. 17, No. 1, p. 84.
- Mosayk (2016) "Using the Applied Element Method to model URM walls subjected to in-plane cyclic shear-compression," Pavia, Italy.
- Mosayk (2017a) "Using the Applied Element Method to model the shake-table testing of two full-scale URM houses," Pavia, Italy.
- Mosayk (2017b) "Using the Applied Element Method to model the collapse shake-table testing of a URM cavity wall structure," Pavia, Italy.
- Mosayk (2017c) "Using the Applied Element Method to model the collapse shake-table testing of a terraced house roof substructure," Pavia, Italy.
- Tomassetti U., Kallioras S., Graziotti F., Correia A. (2017b) "Final report on the construction of the building prototype at the LNEC laboratory," European Centre for Training and Research in Earthquake Engineering (EUCENTRE), Pavia, Italy.